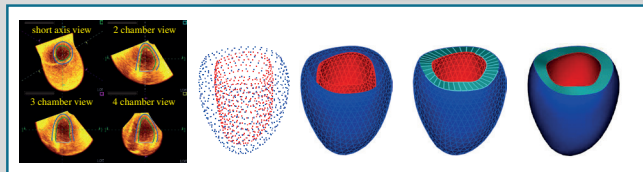
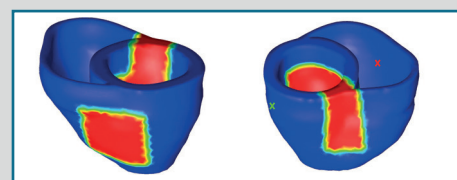
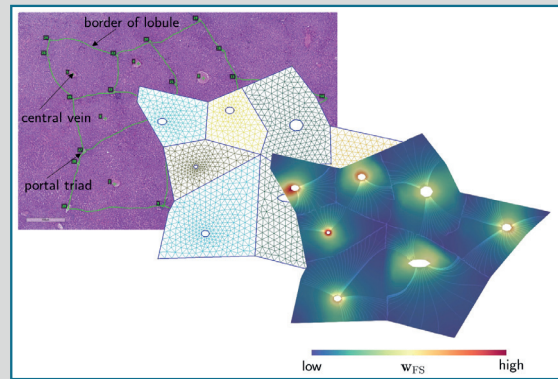


Report

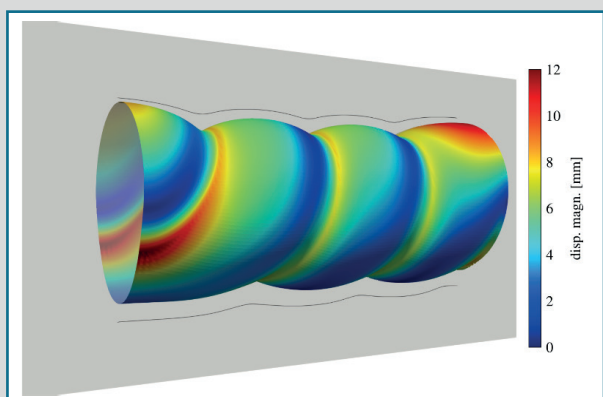
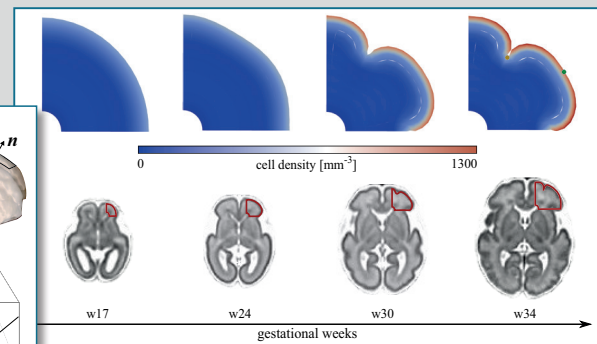
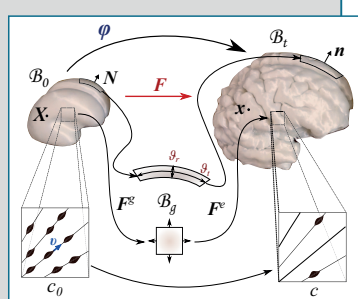
QuaLiPerF - Multi-X Liver Modelling

**TIM RICKEN, LENA LAMBERS, BRUNO CHRIST, UTA DAHLEN,
KARL-HEINZ HERRMANN, MATTHIAS KÖNIG, MANJA MARZ,
NICOLE RADDE, JÜRGEN R. REICHENBACH, LARS OLE SCHWEN,
HANS-MICHAEL TAUTENHAPPN**



Coupling cellular brain development with cortical folding

**SILVIA BUDDAY, MOHAMMAD
SAEED ZARZOR**



Computational Modeling of the Stomach

**ROLAND C. AYDIN, ROUSTEM N. MIFTAHOF, SEBASTIAN
BRANDSTAETER, SEBASTIAN L. FUCHS, CHRISTIAN J. CYRON**



Publisher:

GACM
The German Association for Computational
Mechanics

Address:

Institut für Statik und Dynamik der Tragwerke
Technische Universität Dresden
01062 Dresden
Phone: +49 351-463-35738
Fax: +49 351-463-37086
email: gacm@mailbox.tu-dresden.de
Internet: www.gacm.de

Editor-in-Chief: Michael Kaliske

Guest Editor: Tim Ricken

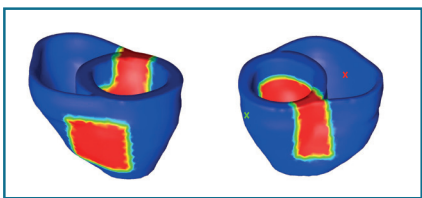
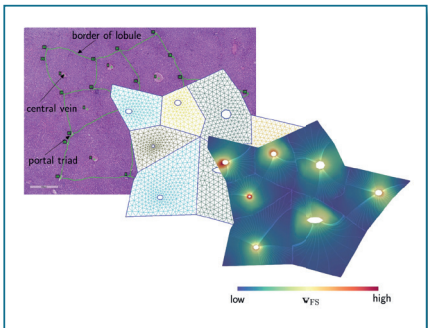
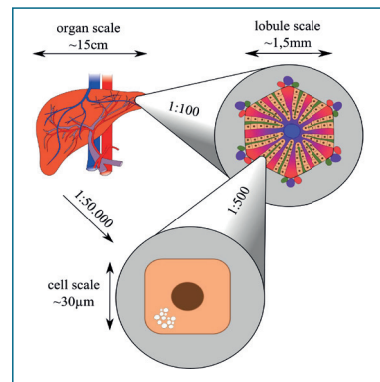
Grafik-Design & Print:

K. Schmidle Druck und Medien GmbH, Ebersberg

Print Run: 450

© 2020 gacm

contents



GACM-News

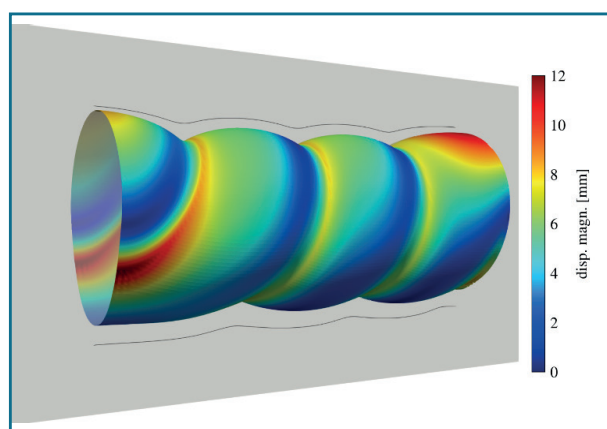
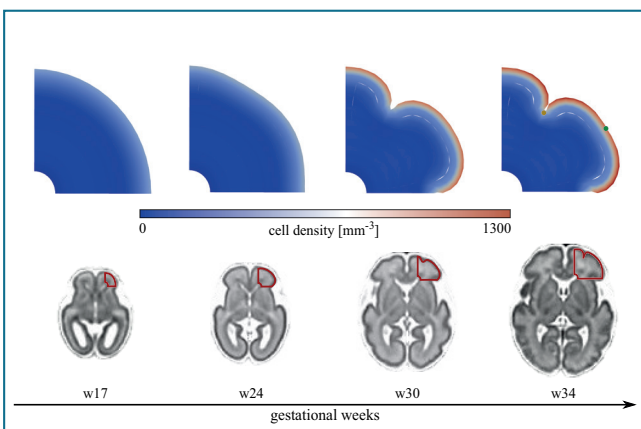
- Editorial 4
- Message of the President 5

Journal

- QuaLiPerF - Multi-X Liver Modelling
TIM RICKEN, LENA LAMBERS, BRUNO CHRIST, UTA DAHMEN,
KARL-HEINZ HERRMANN, MATTHIAS KÖNIG, MANJA MARZ,
NICOLE RADDE, JÜRGEN R. REICHENBACH, LARS OLE SCHWEN,
HANS-MICHAEL TAUTENHAWN 6

- Simulating Clinically Relevant Cases in Cardiology via Numerical Tools
BARIŞ CANSIZ & YONGJAE LEE, LUCAS A. WOODWORTH,
MICHAEL KALISKE 18

- Coupling cellular brain development with cortical folding
SILVIA BUDDAY, MOHAMMAD SAEED ZARZOR 27
- Computational Modeling of the Stomach
ROLAND C. AYDIN, ROUSTEM N. MIFTAHOF,
SEBASTIAN BRANDSTAETER, SEBASTIAN L. FUCHS,
CHRISTIAN J. CYRON 34



Editorial

Special Issue: Computational Continuum Biomechanics

The development in the field of computational simulation based on continuum-biomechanical models has made considerable progress in recent years.

On the one hand, the models and simulations can be used to obtain a deeper insight into the highly complex biochemical-physical coupled processes in living tissues. This usually requires high-resolution and in some cases multi-scale models with a high-fidelity level of detail. The computational effort is correspondingly expensive and high-resolution large-scale calculations can only be performed in parallel on high-performance computers.

On the other hand, the models are already of such high quality that they provide support for therapy decisions in clinical practice. This requires both robust and fast calculation methods. This is the goal of the newly established DFG priority program SPP 2311 "Robust coupling of continuum-biomechanical *in silico* models for active biological systems as a preliminary stage of clinical applications – co-design of modelling, numerics and usability". The aim is to develop solution concepts in the co-design of mechanical modelling, numerical solution and medical issue, which can make a model-based, computer-aided supporting contribution in clinical practice.

This volume presents examples of high-resolution continuum-biomechanical models of the human organs liver, heart, brain and stomach.

The paper "Multi-X Modeling of Complex Biological Systems in Health and Disease Using the Liver as a Showcase" by Tim Ricken, Lena Lambers et al. presents the experiences and challenges of the recently founded Research Unit QuaLiPerF (FOR 5151). The Research Unit deals with the multiscale modelling of the human liver. Special attention is given to the integration of physiological data for liver-specific modelling. To achieve successful modelling, many different disciplines collaborate in QuaLiPerF, including mechanics, bioinformatics, statistics, experimental animal surgery, cell transplantation, radiology and clinical transplantation.

In the article "Simulating Clinically Relevant Cases in Cardiology via Numerical Tools" by Baris Cansiz et al., the authors give an insight on the finite element-based numerical framework for the simulation of the heart. The presented computational model enables an application to real-life situations. Here, the authors examine the impact of different effects, e.g. (de)fibrillation, cardiac resynchronization therapy or the intake of verapamil on the heart beat showing the cardiac cycle as well as snapshots from representative time steps in the simulation.

The contribution "Coupling Cellular Brain Development with Cortical Folding" by S. Budday and M. S. Zarzar deals with the relationship between cellular brain development and cortical folding. The authors investigate the relationship between mechanical instabilities (leading to cortical formations) to gain better insights into various neurological disorders. Mechanical instabilities are closely related to cell migration or cellular connectivity. For this purpose, the authors apply a multi-field computational model (coupling of the advection-diffusion model with finite growth) to the problem. They can thus demonstrate that computer models based on the nonlinear field theories of mechanics are a promising tool to transfer processes on the cellular scale to structural changes on the continuum scale. This approach enables authors to explicitly predict how disturbances at the cellular level affect growth, folding, and structural anomalies at the continuum scale.

The last article "Computational Modeling of the Stomach" by R. C. Aydin et al. gives a short overview of the current state of the art concerning the computational modeling of the gastro-intestinal tract. The authors divided the topic into five parts to highlight possible topics within each area depending on different backgrounds in computational mechanics: elasticity of the gastric wall, electric waves in the gastric wall, active muscle tension in the wall, multi-phase flow of digesta and the fluid-structure interactions.

December 2020
Tim Ricken

Institute of Mechanics, Structural Analysis and Dynamics
Faculty of Aerospace Engineering and Geodesy
University of Stuttgart

Message of the President

The German Association for Computational Mechanics (GACM) would like to draw the attention of the readership of this GACM-Report No. 13 to the challenging and fast developing field of Computational Continuum Biomechanics. Thanks to the efforts of guest editor Professor Tim Ricken, who's dedication is acknowledged, four fascinating manuscripts can be presented illustrating this research. The importance and current momentum of the field is underlined by the fact that the German Research Foundation (DFG) just established a national wide Priority Program SPP 2311 on *Robust Coupling of Continuum-biomechanical In Silico Models to Establish Active Biological System Models for Later Use in Clinical Applications – Co-design of Modelling, Numerics and Usability*, which will further foster the basic research in this field.



Currently, we face in general a challenging situation due to the Covid-19 pandemic. For all of us, life has been dramatically changed during the last months. The academic and scientific life went nearly totally online instead of having large conferences or smaller workshops in presence meeting friends and colleagues. Technically, we could adapt to the new formats relatively fast. Maybe, we even can identify some positive aspects as we do not lose any time in travelling and more people more easily can join the online formats. These meetings are not virtual – they are real – even though online. Surely, we all miss the social components and many facets which are less present in these online gatherings. Nevertheless, for the sake of our safety, we do not have any choice. Maybe our community is naturally more familiar with these formats due to the fact that virtualization is our daily business in computational mechanics. Having nowadays the meeting online gives us additional degrees of freedom, reduces efforts and we can reach more people easily. This experience will help us to develop creative formats for the future.

On 11 December 2020, GACM will hold its regular general assembly including elections – of course online. Thus, we will continue with our efforts for science and research as well as service to the community. About other events and the accompanying formats, members should consult the according web pages for an update.

Looking forward towards the upcoming scientific events and stay healthy. I remain with my best regards

Michael Kaliske, President of GACM

QuaLiPerF – Multi-X Liver Modelling

by Tim Ricken¹, Lena Lambers¹, Bruno Christ², Uta Dahmen³, Karl-Heinz Herrmann⁴, Matthias König⁵, Manja Marz⁶, Nicole Radde⁷, Jürgen R. Reichenbach⁴, Lars Ole Schwen⁸ & Hans-Michael Tautenhahn^{3,9}

¹ Institute of Mechanics, Structural Analysis and Dynamics, Faculty of Aerospace Engineering and Geodesy, University of Stuttgart, Germany

² Cell Transplantation/ Molecular Hepatology Lab, Department of Visceral, Transplant, Thoracic and Vascular Surgery, University of Leipzig Medical Center, Germany

³ Experimental Transplantation Surgery, Department of General, Visceral and Vascular Surgery, Jena University Hospital, Germany

⁴ Medical Physics Group, Institute of Diagnostic and Interventional Radiology, Jena University Hospital, Germany

⁵ Systems Medicine of the Liver Lab, Institute for Biology, Institute for Theoretical Biology, Humboldt-University Berlin, Germany

⁶ RNA Bioinformatics and High-Throughput Analysis, Faculty of Mathematics and Computer Science, Friedrich Schiller University Jena, Germany

⁷ Institute for Systems Theory and Automatic Control, Faculty of Engineering Design, Production Engineering and Automotive Engineering, University of Stuttgart, Germany

⁸ Fraunhofer Institute for Digital Medicine MEVIS, Bremen, Germany

⁹ Department of General, Visceral and Vascular Surgery, Jena University Hospital, Germany

1 Motivation

In this paper we present the objectives regarding multi-X liver modelling of the recently DFG-funded research unit **QuaLiPerF** (Quantifying Liver Perfusion-Function Relationship in Complex Resection – A Systems Medicine Approach). The aim of the research unit (RU) is to elucidate the interactions between the changes in blood flow in the liver, also called perfusion, when normalized on liver volume, and the metabolic function of the liver. It will be investigated how this function-perfusion interaction will be influenced by a liver resection operation and how this knowledge can be used in the clinical practise. On this basis, a model of the perfusion of the liver and its function is to be developed, which in the long term will make it possible to better predict liver function and regeneration after surgery and thus minimize the risk of liver failure, see Figure 1. The challenge of modelling biological systems is that they are by nature highly complex and often difficult to understand. Two main reasons are that biological systems

- i) are developed in an evolutionary process in contrast to deliberate design on a white-board, and that
- ii) they are inherently multiscale and consist of specialized cells that form tissues capable of performing multiple functions.

Thus, multiscale modelling including evolutionary optimisation can contribute to a better understanding of the biology underlying these complex systems.

The simulation can potentially support clinical decision-making based on predictions obtained as simulation output.

Two scenarios are clinically important: to predict the progression of liver disease with and without a given treatment, and to predict the outcome after major removal of liver mass as needed in case of hepatic malignancies. The outcome is dependent on the individual risk of liver failure and the putative course of liver regeneration which is related to the planned type and extent of liver resection and the severity of an eventually underlying disease of the liver, such as steatosis, fibrosis or even cirrhosis and the overall condition of the patient. Thus, the liver is an ideal showcase for complex biological systems.



Figure 1: Surgeon's view on an extended liver resection in human.

2 The Perfusion-Function Interaction

The term “perfusion” refers in general to the passage of blood through the circulatory system to an organ with its capillary bed. Perfusion of the liver is ensured via a dual supply: the portal vein supplying the liver with nutrient-rich blood from the intestine and the hepatic artery, supplying the liver with oxygen-rich blood from the lung. Venous drainage is ensured via the hepatic veins. The main liver cells, called hepatocytes, located along the capillaries, called sinusoids, are supplied with nutrients and oxygen via the blood flow. The liver is the metabolic hub of the body playing a central role in detoxifying substances such as drugs, and metabolism of glucose, amino acids and fats. The term “function” refers to these metabolic processes in the liver cells, e.g. glucose metabolism, fat metabolism or detoxification.

Due to the blood pressure gradient in the organ in combination with cells functioning as sources or sinks, substance gradients are established within the tissue. These gradients and especially the local concentration in the tissue are important factors determining cellular function. The cells in the tissue are specialized to perform certain tasks depending on the local substance concentrations and thus on their position in the gradient. The combination of substance concentration and cell specialization yields complex perfusion-function interactions. In the liver tissue, as an example, a gradient exists in the glucose metabolism with different cell functions depending on the location in the tissue (either glucose producing or glucose consuming). This cell-dependent function can be modulated based on the actual glucose (and other metabolites and hormones) gradients throughout the liver tissue. Perfusion of the tissue is therefore an important driver of organ function.

3 Multiscale Modelling of the Liver

In order to model the liver mathematically, it can be divided into three scales, cf. Figure 2:

- i) organ scale: The liver consists of a blood-supplying and blood-draining vascular perfusion system, which is organized hierarchically and composed of a coarse and fine network of hepatic vessels ($\sim 1\text{--}10$ mm). The supplying system provides the liver with oxygen-rich (via hepatic artery) and nutrient-rich (via portal vein) blood, whereas the draining system disposes of waste products.
- ii) lobule scale: The lobular units ($\sim 1\text{--}1.5$ mm) of the liver (metabolic unit) connect the supplying and draining systems. Arterial and venous blood from the supplying system is mixed, guided along columns (sinusoids) of hepatocytes (liver cells), and removed through the central vein into the draining system. The interaction between mixed blood and hepatocytes forms the functional unit of the liver.
- iii) cell scale: The hepatocytes ($\sim 10\text{--}30$ μm) ingest oxygen and nutrients and deplete waste products. They are responsible for detoxification, protein-synthesis and metabolic homeostasis.

A fourth scale not directly related to the liver but relevant for the perfusion input and output is required: The whole-body scale, which embeds the liver into the systemic circulation of the whole-body.

To capture the organ physiology and interaction including the hepatic metabolism, a multiscale approach is required. Thus, detailed mathematical models on the different scales and an efficient modelling coupling are essential. In order to map the complex biological interactions and constraints, physiological data are necessary, which are integrated into the models via data integration methods.

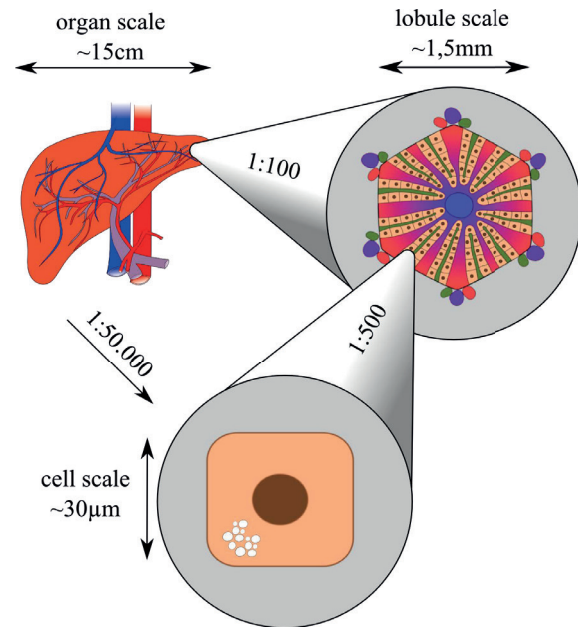


Figure 2: Different size scales of the human liver.

3.1 Modelling Approach on Organ Scale

The first one of maybe four branching levels of the vascular architecture of the human liver can be determined by *in vivo* CT scans with a resolution of several hundred micrometers. To determine the underlying branching levels, optimization algorithms have been developed that artificially generate the underlying levels starting from the upper vessel structures, see e.g. KÖPPL ET AL. [29] or SCHWEN ET AL. [58]. Based on this geometrical data, mostly 1D blood flow simulations are performed to mimic e.g. the transient blood, nutrient and oxygen distribution.

In addition, MRI, sonography and elastography are available to obtain information on the upper liver scale at organ level. For example, the bioMMeda research group of Segers and Debbaut has developed a method to

segment and analyze the morphological and geometric data of liver-vascular trees based on imaging data such as CT or MRI ([2], [4]). In addition to these structural data, sonography will provide blood flow measurements at the liver entrances and exits, while elastography will provide data on the mechanical properties of the liver, such as the stiffness of liver tissue.

3.2 Modelling Approach on Lobular Scale

A promising approach to model the complex biological structure of the lobular tissue with its macroscopic blood flow and nutrient transport is offered by the homogenization approach based on the Theory of Porous Media (TPM), cf. EHLERS [15] and DE BOER [5]. To describe the hepatic function-perfusion processes in the liver lobules, RICKEN ET AL. [53, 51, 50] developed a multicomponent, poro-elastic multiscale and multiphase model based on the TPM. The total body φ consists of three phases φ^α , namely the healthy liver tissue φ^S , fat tissue φ^T and blood φ^F . Since the model also takes into account the description of solute components responsible for the metabolic processes on the cellular scale, the extended Theory of Porous Media (eTPM) can be used according to RICKEN ET AL. [52], where the body φ consists of carrier phases φ^α and the microscopic substances $\varphi^{\alpha\beta}$:

$$\varphi = \sum_{\alpha=1}^{\kappa} \varphi^\alpha := \sum_{\alpha=1}^{\kappa} \left[\sum_{\beta=1}^{\nu-1} (\varphi^{\alpha\beta}) + \varphi^\alpha \right] \quad (1)$$

To account for the growth or regression of fat tissue $\hat{\rho}^\alpha$, dependent on a biochemical activity, we utilize a mathematical model developed by SCHLEICHER ET AL. [57]. It describes hepatic lipid dynamics to simulate the development of fatty acids in hepatocytes. The model includes fatty acid uptake, lipid oxidation and lipid export.

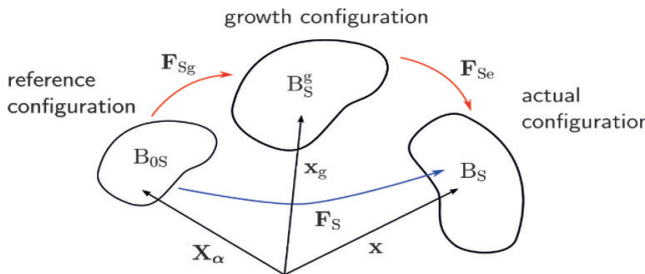


Figure 3: Growth approach according to RODRIGUEZ[54].

The resulting tissue growth is implemented using a multiplicative split of the deformation gradient \mathbf{F}_S into an elastic part \mathbf{F}_{Se} and a growth part \mathbf{F}_{Sg} according to RODRIGUEZ [54], cf. Figure 3, with

$$\mathbf{F}_S = \mathbf{F}_{Se} \mathbf{F}_{Sg}. \quad (2)$$

This leads to the growth part of the deformation gradient using the multiplicative split in combination with the multiphase theory, cf. WERNER [61], with

$$\begin{aligned} \mathbf{F}_{Sg} &= (J_{Sg})^{1/3} \\ J_{Sg} &= \exp \left(\int \hat{n}^T dt \right). \end{aligned} \quad (3)$$

Evaluating the balance of momentum for the fluid, the seepage velocity $n^F \mathbf{w}_{FS}$ is determined with

$$\mathbf{n}^F \mathbf{w}_{FS} = \mathbf{K}_F [-\operatorname{grad} \lambda], \quad (4)$$

cf. PIERCE ET AL. [43], wherein \mathbf{K}_F with

$$\begin{aligned} \mathbf{K}_F &= (n^F)^2 \mathbf{R}_F^{-1} = k_{0S} \left(\frac{n^F}{1 - n_{0S}^S} \right)^m \mathbf{M}^*, \\ \mathbf{M}^* &= \kappa \mathbf{I} + \frac{(1 - 3\kappa)}{I_4} \mathbf{M} \end{aligned} \quad (5)$$

is a positive definite material parameter tensor representing the intrinsic hydraulic resistance of the cartilage solid. In liver tissue, the permeability depends on the deformation and is characterized using the initial Darcy permeability k_{0S} [m^4/Ns] and m , a dimensionless material parameter controlling the general isotropic deformation dependence of the permeability. Inclusion of the volume fraction n^F relates to the change of permeability caused by the change of pore space, where n_{0S}^S denotes the reference solid volume fraction. The (spatial) structural tensor \mathbf{M} is defined as $\mathbf{M} = \mathbf{a} \otimes \mathbf{a}$ wherein \mathbf{a} represents the preferred blood flow direction given by the sinusoids. Beside the tensor of identity \mathbf{I} , we use κ to define the range of permeabilities resulting from ideal alignment sinusoids ($\kappa = 0$) to an isotropic distribution of the sinusoids ($\kappa = 1/3$). This approach enables the detection of blood flow distribution in segmented groups of liver lobules, cf. Fig. 4.

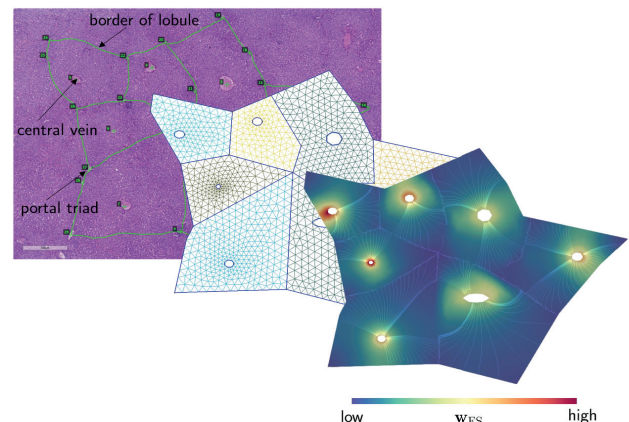


Figure 4: Segmentation, meshing and simulation of hepatic blood flow using a group of liver lobules segmented from a histological image.

Solving the resulting degrees of freedom set \mathcal{R} remains with

$$\mathcal{R} = [\mathbf{u}_S, p^{FR}, n^S, n^T, \mu^{\alpha\beta}], \quad (6)$$

For the numerical treatment, weak formulations of the governing equations based on the balance relations are formed within the framework of a standard GALERKIN procedure as evaluated e.g. in WERNER [61]:

- Balance of momentum for the mixture:

$$\int_{B_S} \{ \mathbf{T} \operatorname{grad} \delta \mathbf{u}_S \} dv = \int_{\partial B_S} \{ \mathbf{t}_0 \delta \mathbf{u}_S \} da \quad (7)$$

- Balance of mass for the mixture:

$$\int_{B_S} \left\{ \operatorname{div}(n^F \mathbf{w}_{FS}) + \operatorname{div} \mathbf{x}'_S - \hat{\rho}^T \frac{1}{\rho^{TR}} \right\} \delta p^{FR} dv = 0 \quad (8)$$

- Balances of mass for the solid tissue and the fat tissue:

$$\int_{B_S} \left\{ (n^S)'_S \delta n^S + n^S \operatorname{tr} \mathbf{D}_S \delta n^S \right\} dv = 0 \quad (9)$$

$$\int_{B_S} \left\{ (n^T)'_S \delta n^T + n^T \operatorname{tr} \mathbf{D}_S \delta n^T - \frac{\hat{\rho}^T}{\rho^{TR}} \delta n^T \right\} dv = 0 \quad (10)$$

- Balance of mass for the solutes in the solid tissue:

$$\int_{B_S} \left\{ n^S (c^{S\beta})'_S \delta \mu^{S\beta} + c^{S\beta} (n^S)'_S \delta \mu^{S\beta} + n^S c^{S\beta} \mathbf{D}_S \cdot \mathbf{I} \delta \mu^{S\beta} - \frac{\hat{\rho}^{S\beta}}{M_{mol}^\beta} \delta \mu^{S\beta} \right\} dv = 0 \quad (11)$$

- Balance of mass for the solutes in the fluid phase:

$$\int_{B_S} \left\{ n^F (c^{F\beta})'_S \delta \mu^{F\beta} + \operatorname{div} \mathbf{j}_{F\beta S} + c^{F\beta} (n^F)'_S \delta \mu^{F\beta} + n^F c^{F\beta} \mathbf{D}_S \cdot \mathbf{I} \delta \mu^{F\beta} - \frac{\hat{\rho}^{F\beta}}{M_{mol}^\beta} \delta \mu^{F\beta} \right\} dv = 0 \quad (12)$$

The results in Figure 5 illustrate i) a group of healthy liver lobules (left) and ii) an outflow obstruction in one lobule with the respective inflow (red) and outflow (blue) boundary conditions (right). The resulting change in perfusion alters the function of the liver cells and thus the accumulation of fat represented by a change in volume fraction of fat tissue n^T , cf. Figure 5 b).

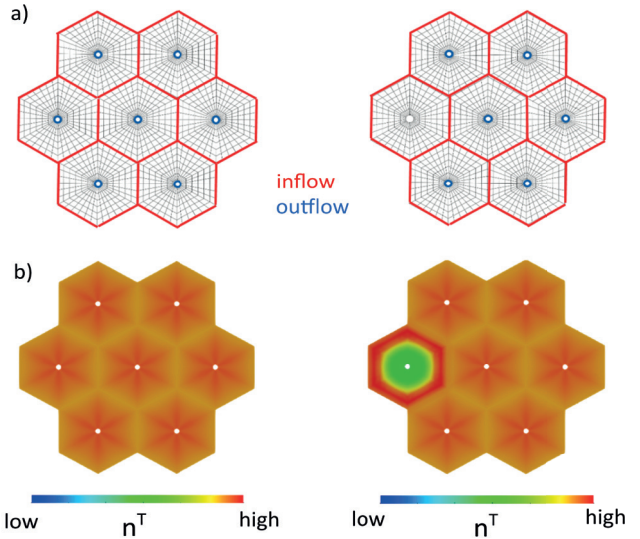


Figure 5: a) boundary value problem representing a healthy group of lobules on the left and an obstructed outflow on the right, b) spatial distribution of fat volume fraction n^T , cf. LAMBERS ET AL. [35].

3.3 Modelling Approach on Cellular Scale

For modelling the hepatic function on the cellular scale, the most important processes are metabolism (synthesis, degradation, and transformation of biological molecules), and signal transduction (processing and transfer of information based on biological molecules). The objective of metabolic modelling is to understand how metabolites are interconverted and to determine the rates at which these transformations take place in the cell. Main building blocks of such metabolic models are metabolites (and proteins), the metabolic reactions catalyzing the conversion of these metabolites, and the genes which encode the reactions. To model metabolism, the two main approaches are: (i) steady-state-based methods, the most popular being Flux Balance Analysis [40], and (ii) dynamic approaches based on ordinary differential equations (ODE).

A global view of the metabolic capabilities of a cell can be obtained via genome-scale metabolic models (GEMs), consisting of a comprehensive collection of metabolites, reactions and genes of a given cell. GEMs allow to analyze the flow of metabolites through the network using flux balance analysis (FBA) and similar algorithms. Multiple GEMs of the liver exist [17, 22, 1, 38] and have been applied to study central metabolic functions of the liver [17] or the effects of deletions of single enzymes [41]. To model the metabolism dynamically, kinetic pathway models based on ordinary differential equations (ODE) are used. This approach focuses on specific metabolic functions and pathways by means of detailed mathematical description of the involved cellular processes and molecular players, cf. Figure 6. These ODE models allow to simulate the time evolution of the system, providing a dynamic understanding of the

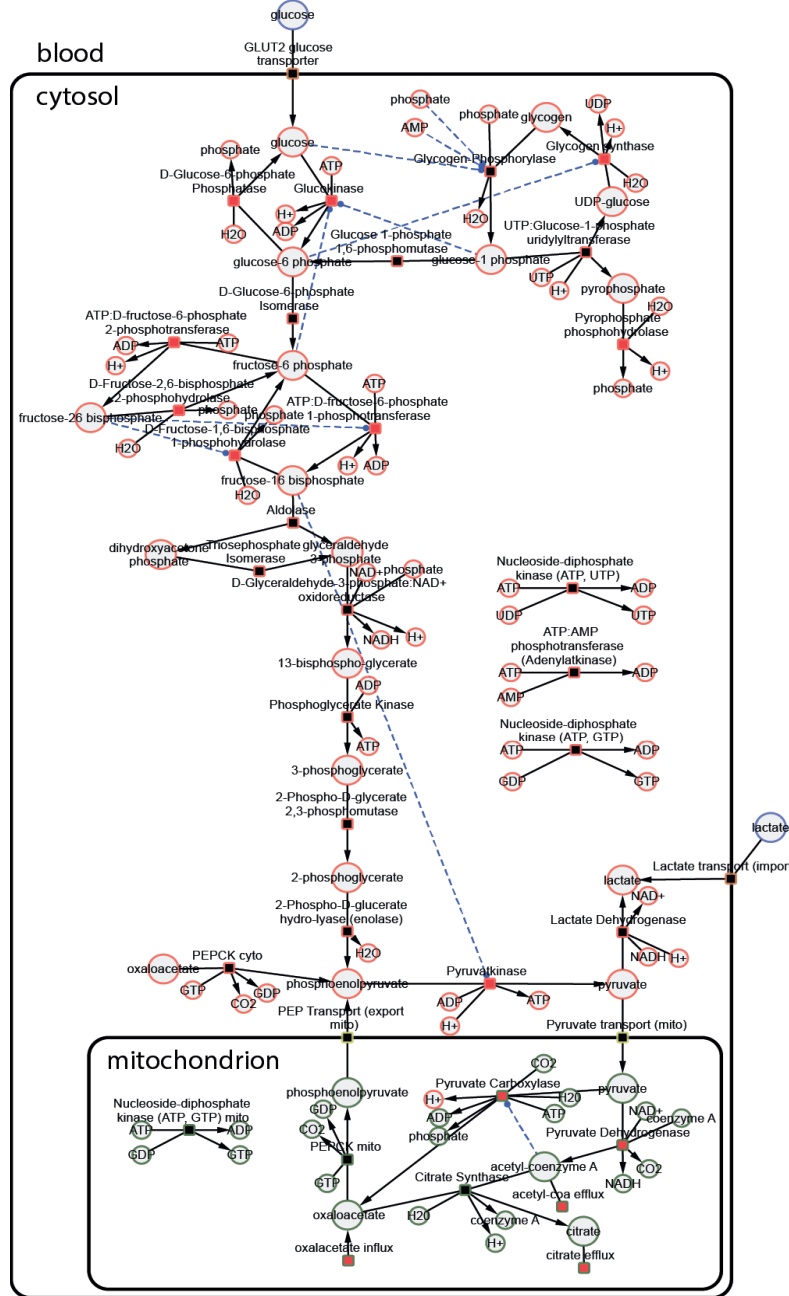
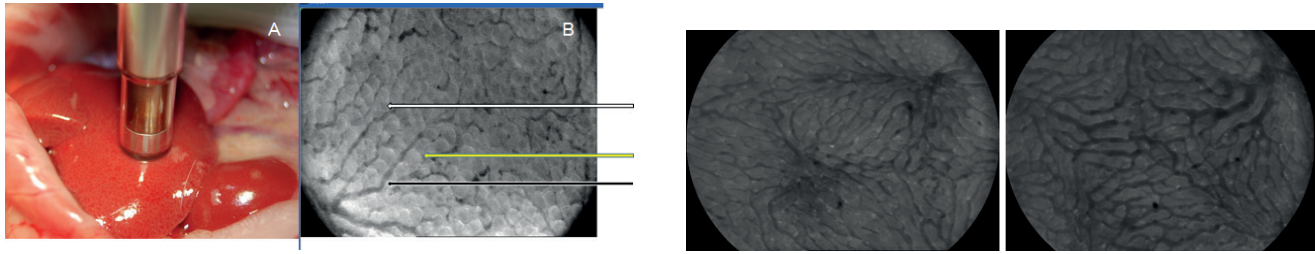


Figure 6: Metabolic model of hepatic glucose metabolism, KOENIG [28], consisting of metabolites and reactions which catalyze the conversions.

involved processes. Kinetic pathway models of central liver functions have been developed, e.g., a minimal model of lipid metabolism in steatosis development [56] or models for the detoxification of substances by the liver such as paracetamol [49]. We developed detailed kinetic models of human hepatic glucose homeostasis [25, 26] providing insights into the switch between glucose production and utilization by the liver depending on hormonal regulation by insulin and glucagon. Recently, this kinetic model was extended substantially to cover the central carbon metabolism of the liver (HepatoKin1) [4]. To describe signal transduction, the two main approaches are boolean networks and ODE models. The main goal hereby is to understand how

external signals (often hormones) are transduced in changes in cellular state and behavior. Main building blocks in signalling models are (i) changes of activity of enzymes via protein modifications such as phosphorylation; (ii) complex formation of signalling molecules; (iii) changes in transcription (with subsequent changes in proteins). A variety of mathematical models of hepatic signaling processes were developed, using ordinary differential equations (ODEs) or boolean approaches. E.g., signalling models exist for the origin of zonation patterns by the Wnt/ β -catenin signaling pathway [27] or the link between hepatic metabolism and the circadian clock [62].



a) Assessment of microcirculation in a steatotic rat liver. Note the difference in sinusoidal diameter. **A** Sensor on hepatic surface. **B** Hepatic lobule: white arrow points to compressed sinusoid, black arrow to dilated sinusoid, yellow to fat-laden hepatocyte.

b) Assessment of microcirculation using orthogonal polarization spectroscopy before (image on left side) and after 70% partial hepatectomy (image on right side). Note the difference in sinusoidal diameter.

Figure 7: Assessment of microcirculation.

For a recent review of hepatic models of metabolism and signalling relevant in the context of liver surgery, we refer to [9].

4 Data-integrated Modelling

The importance of data in simulation science has increased in recent years. The realistic simulation of physiologic processes requires a detailed knowledge of the underlying processes and the impact of changed simulation boundaries. Models take initial values for certain physical parameters such as initial concentrations of metabolites, blood pressure or fat accumulation, the variance of which can lead to a large deviation of model predictions from the measured biological process. Furthermore, the models must be validated in order to verify their use for experimental and clinical applications.

In liver modelling, perfusion data as well as the spatial distribution of zonated processes in liver lobules and cells are important inputs for model parameterization and validation.

4.1 Perfusion Data

Hepatic perfusion is distributed heterogeneously throughout the liver under normal conditions and even more in case of focal hepatic tumors and after hepatic surgery as well as in global disease states such as hepatic steatosis (fatty liver disease).

A liver tumor may lead to the compression of larger vessels leading to compromised hepatic perfusion on the organ scale. Liver resection, the removal of hepatic parenchyma together with the corresponding vascular bed, leads to portal hypertension and portal hyperperfusion of the remnant organ. Hyperperfusion causes dilation of the majority of sinusoids and compression of the remaining ones, leading to heterogeneous perfusion of the remnant liver on the lobular scale.

Steatosis, the accumulation of fat droplets in hepa-

tocytes, is also causing perfusion irregularities on the lobular scale. The fat droplets are causing compression of the majority of hepatic sinusoids on the one hand, and, on the other hand, dilation of the remaining ones. Both together lead to inhomogeneous perfusion of the organ and compromise hepatic perfusion and subsequently metabolic function.

Therefore, global as well as spatially resolved assessment of hepatic perfusion on the organ scale but also on the microscopical scale is needed. Global hepatic perfusion is assessed by determination of hepatic hemodynamics: assessment of portal pressure ($\text{cm H}_2\text{O}$) as well as hepatic arterial blood flow, portal flow velocity (m/s) and flow rate (ml/s). Spatially resolved assessment of hepatic perfusion on the organ scale is based on imaging technologies such as CT and MRI. However, currently only a low spatial resolution is achieved.

In contrast, determination of hepatic microcirculation is limited to the visualization and quantification of hepatic perfusion in single hepatic lobules using e.g. orthogonal polarization spectroscopy, cf. Figure 7. Assessment of the perfusion heterogeneity requires multiple measurements on selected single spots of the liver surface. Here, parameters such as the relative percentage of perfused hepatic sinusoids and the sinusoidal blood flow can be determined. These parameters can be determined under different experimental and clinical conditions and are needed as input data for modelling.

4.2 Zonation Data

In the liver, metabolic functions are also distributed heterogeneously in the tissue. E.g., gluconeogenesis (glucose production) is predominantly executed by hepatocytes surrounding the regions of the portal vein (periportal), while glycolysis (glucose consumption) is predominantly executed by hepatocytes surrounding the central vein (pericentral). This functional heterogeneity was termed metabolic zonation and was attributed to blood-born nutrient, hormone, and morphogen gradients, cf. JUNGERMANN AND KATZ [23]. These

gradients form in the blood streaming along the hepatic sinusoids, the most terminal branches of the portal vein at the entry, and the most terminal branches of the central vein at the exit site of the sinusoid. Likewise, adhesion proteins involved in the formation of cell-cell contacts, which are necessary for the proper epithelial organization of the hepatic parenchyma, are distributed zonally. These proteins, comprising cadherins and others, cf. Figure 8, determine the epithelial orientation of the hepatocyte and thus contribute to the functional features of the hepatocyte. Impairment of cell-cell contacts in liver diseases like non-alcoholic steatohepatitis abrogates the zonal distribution of metabolic functions indicating a structure-function relationship between adhesion proteins and metabolic regulation, cf. HEMPEL [19].

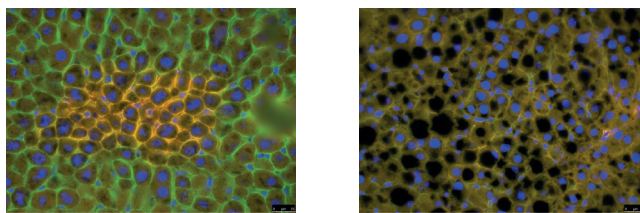


Figure 8: Zonation of adhesion proteins in the liver. E-cadherin (left, yellow) is expressed in periportal hepatocytes, while N-cadherin (left, green) is expressed pan-parenchymally. Under pathological conditions like fatty liver disease, the zonal pattern of adhesion proteins is abrogated (right, black “holes” represent lipid droplets).

Carbohydrate metabolism in hepatocytes is regulated under physiological conditions by the glucoregulatory hormones insulin and glucagon. Isolated hepatocytes in cell culture respond to insulin and glucagon with glucose utilization and production, respectively, which in the intact parenchyma is a predominant feature of pericentral and periportal subpopulations of hepatocytes, cf. CHRIST [8]. This indicates that the specification of hepatocytes might be independent of their position in the sinusoid per se. Moreover, the hepatocyte metabolic response is dynamic, which corroborates that blood-borne gradients specify hepatocyte functions rather than their sinusoidal positioning. It is self-evident that gradient formation in the sinusoidal blood stream might change with modifications in perfusion conditions. However, the biological processes coupling perfusion and metabolism are unknown so far. Hence, it would be feasible to assume a quantitative relationship between the two, implying that perfusion changes dynamically impact on metabolic changes, causing a proportional response. Integration of perfusion and metabolism in computational simulations might elucidate how these are connected. In addition, identification of biological pathways involved might also shed light on the molecular mechanisms translating extracellular perfusion changes into an adequate metabolic response by the hepatocyte. Best candidates to achieve this coupling might be molecular mechanosensors on the hepatocyte

surface including adhesion proteins like cadherins.

4.3 MRI Data

Magnetic resonance imaging (MRI) provides spatially resolved, multi-parametric quantitative *in vivo* information of the liver. This ranges from anatomical information, like liver volume [44, 10] or diet-based inhomogeneous fat enrichment in the tissue [12, 32, 3], to functional assessments using contrast agent excretion or direct flow [7] and perfusion MRI measurements [46, 6]. Differences between various experimental conditions in animal models can be analysed in detail. The main advantages of MRI is its non-invasiveness and scalability between small animal models (rodents) and humans [13, 21]. Once an MRI method is established either clinically or pre-clinically in an animal model, in most cases the MRI method (or sequence) can be quickly translated to the respective other scale. MRI is also able to connect spatial scales as it can reach all the way from a whole human body over rodent body down to organs and further into highly resolved structural and functional data of organ tissue. The current limitations are typically two orders of magnitude above histological cellular resolution but can sometimes be pushed for special cases and methods [13]. MRI can also offer some insights into tissue microstructure by indirectly measuring tissue parameters, which are linked to the microstructure, at a lower spatial resolution.

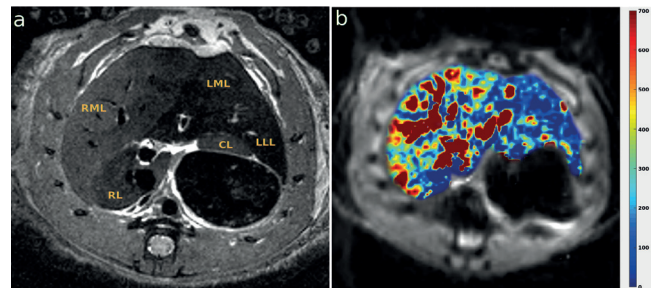


Figure 9: **a)** Anatomical T2-weighted image of a rat with 60% portal vein ligation, which allows normal flow to the right median and caudate lobe and cuts off the portal blood flow to the left and inferior right lobes. Hyper- (lighter grey) and hypo-perfused (darker grey) areas in the different portal supply zones are clearly visible in the anatomical image. The letter abbreviations identify the liver lobes: right median lobe (RML), right lobe (RL), left median lobe (LML), left lateral lobe (LLL), upper caudate lobe (CL). **b)** Position-matched perfusion map derived from a FAIR Spinecho EPI measurement for comparison (color bar: 0-700 ml per 100 g tissue per min). The sharp boundary between hyper perfused (in green and red color) and hypo perfused (mostly blue) liver areas is clearly visible in the quantitative perfusion map. Both images were acquired on a 9.4 T small animal MR system.

Two prominent examples are water diffusion restricted by cell boundaries and tissue perfusion [59, 36, 14],

which both gain information on structures below the current direct spatial resolving power of MRI.

The obtained data give an insight into the systemic *in vivo* adaptations after different surgical interventions, e.g., portal vein ligation or the regenerative response of the remnant liver after resection, cf. Figure 9. Furthermore, with help of the MRI data a comparison of predicted temporal changes provided by the mathematical model is possible.

4.4 Transcriptome Data

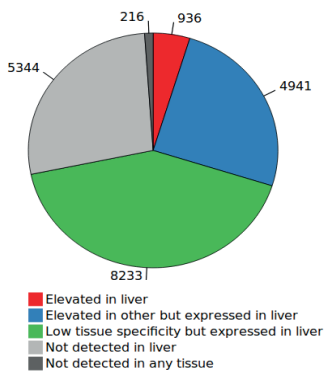


Figure 10: The distribution of all protein-coding genes across the five categories based on transcript specificity in the liver as well as in all other tissues.

The number of genes in the human genome is not entirely determined yet because the number of different isoforms and also the function of numerous transcripts remains unclear. This is especially true for non-coding RNA. The number of protein-coding genes is better known, but varies by 1,400 questionable genes[42, 18, 11, 39]. Transcriptome analysis shows that 72% of all human proteins are expressed in the liver and 936 of these genes show an elevated expression in the liver compared to other tissue types, cf. Figure 10.

Although only a fraction of liver-specific ncRNAs are known, here we summarize important examples of ncRNA participating in the pathogenesis of different forms of liver disease and how they can be used as therapeutic tools or targets for novel treatment paradigms, following the suggestions of ROY ET AL. [55]. In previous works, we analyzed the number of differentially expressed genes across several species and organs. These plots summarize protein-coding genes and non-coding RNA genes. A large number of genes being involved in metabolic processes, inflammation and immune response are differentially expressed during aging, which we expect to see based on our experience of senescence and inflammation in mouse liver [2].

Alterations in protein expression directly affect hepatic metabolism and consequently liver function.

4.5 Data Integration and Uncertainty Quantification

In order to build predictive models for the liver, expert knowledge and experimental data have to be taken into account. However, the integration of data into quantitative and dynamic models on different scales poses several challenges.

(i) First, we often face the sparse data setting problem. Even if model equations can be defined, e.g. for parts of the metabolic network, the data available for model calibration do often not contain enough information to estimate all model parameters uniquely [33, 47]. This is e.g. because only few components of the network are quantified, which results in ill-posed optimization problems [45]. Different approaches exist to deal with this problem, including regularization techniques [33], identifiability analyses [47, 20, 48] and Bayesian approaches [16, 24]. The latter generally allow for a consistent tracking of uncertainty from variability in input data via uncertainty in model parameters to confidence bounds in model predictions, but are computationally expensive.

(ii) Thus, computational costs pose a second challenge for data integration. Sampling approaches, which allow to investigate uncertainty in terms of probability distributions in a Bayesian setting, have to be optimized and adapted to be applicable to larger models. This can be achieved in different ways, including efficient sampling schemes [30], likelihood-based approaches [31] and fast forward simulation times. The latter can be reached by model reduction techniques, e.g. surrogate models via machine learning techniques. This challenge applies to metabolic models and models on the organ scale that are described with ordinary differential equations, but particularly to simulation-intensive models which include spatial resolution such as metabolic zonation or anisotropic blood flow on the lobule scale.

(iii) Standard methodology for the generation of patient-specific models is missing. The integration of blood profiles or liver function tests of individual patients into models requires the development of suitable methodology [60]. Moreover, since post-operative regeneration courses and the risk of liver failure also depend on factors such as gender, age, weight or comorbidities, the integration of these factors into risk assessment is also important.

5 Machine Learning

The simulation of hepatic processes using high-fidelity models requires computational resources to achieve a real-time analysis, e.g., a quick examination of the effects of parameter changes on model outputs. Therefore, artificial neural networks (ANNs) are developed and can be used for model order reduction. To insert a huge

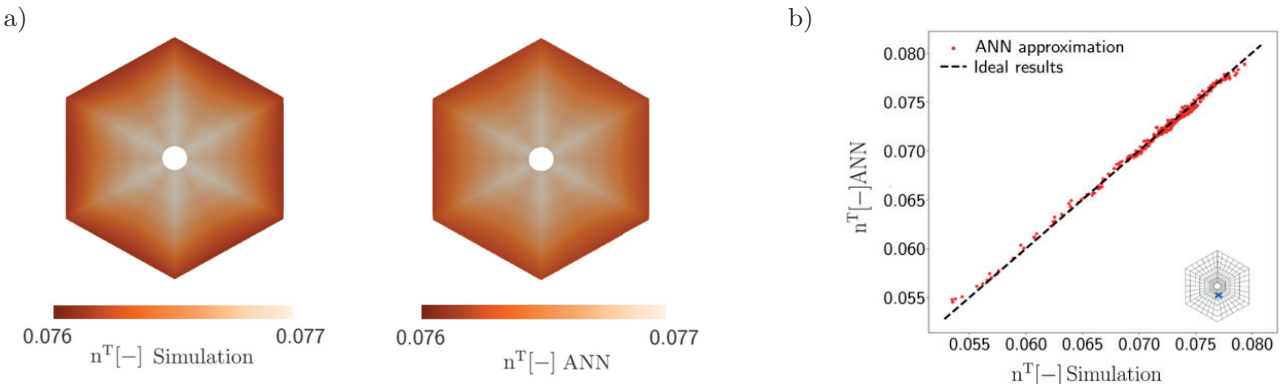


Figure 11: a) Comparison of fat volume fraction calculated using numerical simulation or ANNs. b) Relation between simulated and predicted results of fat volume fraction, cf. LAMBERS ET AL. [34].

amount of experimental and clinical data into the numerical model, ANNs will be trained on a huge amount of data and implemented in the model for the calculation of the rates $\hat{\rho}^\alpha$ in each Gauss-point. As a showcase, we developed a model-free approach to predicting fat volume fraction in the liver lobule at each node in the finite element mesh using ANNs, where sensible hyperparameters (number of layers, number of neurons, loss function, activations,...) were determined using grid search (cf. MIELKE & RICKEN [37] and LAMBERS ET AL. [34]). The results of the spatial distribution of fat volume fraction in the liver lobule in simulation and using ANNs are shown in Figure 11 a). The predicted results are comparable to the simulation results and the relative error is $\leq 1.2\%$. Figure 11 b) illustrates the accuracy of the approximation by comparing the results from simulation and ANN at one point in the liver lobule. The difference between both results is extremely low and the approximation via ANNs fits the ideal results for fat accumulation. The biggest error occurs in the area of small fat accumulation, as the amount of data provided here is significantly lower and therefore less training data is available for this area.

6 Discussion and Conclusion

Understanding liver function requires a multiscale approach bringing together expertise from multiple fields. Therefore, a close cooperation between research in the field of live science, modelling, data integration and the clinical studies will significantly improve the understanding of the complex function-perfusion relationship necessary for the clinical application.

7 Acknowledgement

Funded by Deutsche Forschungsgemeinschaft (DFG, German Research Foundation) under Germany's Excellence Strategy – EXC 2075 – 390740016.

This work was supported by the German Research Foundation (DFG) within the Research Unit Pro-

gramme FOR 5151 "QuaLiPerF (Quantifying Liver Perfusion–Function Relationship in Complex Resection—A Systems Medicine Approach)" by grant number 436883643. MK is supported by the Federal Ministry of Education and Research (BMBF, Germany) within the research network Systems Medicine of the Liver (LiSyM, grant number 031L0054).

References

- [1] R. Agren et al. "Identification of anticancer drugs for hepatocellular carcinoma through personalized genome-scale metabolic modeling." In: *Molecular systems biology* 10 (Mar. 2014), p. 721. ISSN: 1744-4292. DOI: 10.1002/msb.145122.
- [2] E. Barth et al. "Conserved aging-related signatures of senescence and inflammation in different tissues and species". In: *Aging (Albany NY)* 11.19 (2019), p. 8556.
- [3] J. Berglund et al. "Fat/water separation in k-space with real-valued estimates and its combination with POCS". en. In: *Magn Reson Med* 83.2 (Feb. 2020), pp. 653–661. ISSN: 0740-3194, 1522-2594. DOI: 10.1002/mrm.27949. URL: <https://onlinelibrary.wiley.com/doi/abs/10.1002/mrm.27949> (visited on 01/24/2020).
- [4] N. Berndt et al. "HEPATOKIN1 is a biochemistry-based model of liver metabolism for applications in medicine and pharmacology." In: *Nature Communications* 9 (1 June 2018), p. 2386. ISSN: 2041-1723. DOI: 10.1038/s41467-018-04720-9.
- [5] R. de Boer. *Theory of Porous Media – highlights in the historical development and current state*. Berlin: Springer-Verlag, 2000.
- [6] M Chouhan, R Ramasawmy, and A Campbell-Washburn. "Measurement of bulk liver perfusion: initial assessment of agreement between ASL and phase-contrast MRI at 9.4T". In: *Proc Intl Soc Mag Reson Med*. 21 (2013), p. 2190.

- [7] M. D. Chouhan et al. “Use of Caval Subtraction 2D Phase-Contrast MR Imaging to Measure Total Liver and Hepatic Arterial Blood Flow: Preclinical Validation and Initial Clinical Translation”. en. In: *Radiology* 280.3 (Sept. 2016), pp. 916–923. ISSN: 0033-8419, 1527-1315. DOI: 10.1148/radiol.2016151832. URL: <http://pubs.rsna.org/doi/10.1148/radiol.2016151832> (visited on 01/24/2020).
- [8] B. Christ, I. Probst, and K. Jungermann. “Antagonistic regulation of the glucose/glucose 6-phosphate cycle by insulin and glucagon in cultured hepatocytes”. In: *The Biochemical journal* 238.1 (1986), pp. 185–191. ISSN: 0264-6021. DOI: 10.1042/bj2380185.
- [9] B. Christ et al. “Computational Modeling in Liver Surgery.” In: *Frontiers in Physiology* 8 (2017), p. 906. ISSN: 1664-042X. DOI: 10.3389/fphys.2017.00906.
- [10] M. D. Cockman, D. A. Hayes, and B. R. Kuzmak. “Motion suppression improves quantification of rat liver volume in vivo by magnetic resonance imaging”. en. In: *Magn. Reson. Med.* 30.3 (Sept. 1993), pp. 355–360. ISSN: 07403194, 15222594. DOI: 10.1002/mrm.1910300313. URL: <http://doi.wiley.com/10.1002/mrm.1910300313> (visited on 01/24/2020).
- [11] F. Cunningham et al. “Ensembl 2019”. In: *Nucleic acids research* 47.D1 (2019), pp. D745–D751.
- [12] W. T. Dixon. “Simple proton spectroscopic imaging.” en. In: *Radiology* 153.1 (Oct. 1984), pp. 189–194. ISSN: 0033-8419, 1527-1315. DOI: 10.1148/radiology.153.1.6089263. URL: <http://pubs.rsna.org/doi/10.1148/radiology.153.1.6089263> (visited on 01/24/2020).
- [13] B. Driehuys et al. “Small Animal Imaging with Magnetic Resonance Microscopy”. en. In: *ILAR J* 49.1 (Jan. 2008), pp. 35–53. ISSN: 1084-2020. DOI: 10.1093/ilar.49.1.35. URL: <https://academic.oup.com/ilarjournal/article-lookup/doi/10.1093/ilar.49.1.35> (visited on 01/24/2020).
- [14] G. Duhamel et al. “High-resolution mouse kidney perfusion imaging by pseudo-continuous arterial spin labeling at 11.75T: Mouse Kidney Perfusion Measurement with pCASL”. en. In: *Magn. Reson. Med.* 71.3 (Mar. 2014), pp. 1186–1196. ISSN: 07403194. DOI: 10.1002/mrm.24740. URL: <http://doi.wiley.com/10.1002/mrm.24740> (visited on 01/24/2020).
- [15] W. Ehlers. “Foundations of multiphasic and porous materials”. In: *Porous Media*. Springer, 2002, pp. 3–86.
- [16] A. Gelman et al. *Bayesian data analysis*. 2nd ed. Texts in Statistical Science. Chapman & Hall, CRC, 2004.
- [17] C. Gille et al. “HepatoNet1: a comprehensive metabolic reconstruction of the human hepatocyte for the analysis of liver physiology.” In: *Molecular Systems Biology* 6 (Sept. 2010), p. 411. ISSN: 1744-4292. DOI: 10.1038/msb.2010.62.
- [18] J. Harrow et al. “GENCODE: the reference human genome annotation for The ENCODE Project.” eng. In: *Genome Res* 22.9 (2012), pp. 1760–1774. DOI: 10.1101/gr.135350.111. URL: <http://dx.doi.org/10.1101/gr.135350.111>.
- [19] M. Hempel et al. “Pathological implications of cadherin zonation in mouse liver”. In: *Cellular and molecular life sciences : CMLS* 72.13 (2015), pp. 2599–2612. DOI: 10.1007/s00018-015-1861-y.
- [20] S. Hengl and C. Kreutz. “Data-based identifiability analysis of non-linear dynamical models”. In: *Bioinformatics* 23.19 (2007), pp. 2612–18.
- [21] C. Hoyer et al. “Advantages and Challenges of Small Animal Magnetic Resonance Imaging as a Translational Tool”. en. In: *Neuropsychobiology* 69.4 (2014), pp. 187–201. ISSN: 0302-282X, 1423-0224. DOI: 10.1159/000360859. URL: <https://www.karger.com/Article/FullText/360859> (visited on 01/24/2020).
- [22] L. Jerby, T. Shlomi, and E. Ruppin. “Computational reconstruction of tissue-specific metabolic models: application to human liver metabolism.” In: *Molecular systems biology* 6 (Sept. 2010), p. 401. ISSN: 1744-4292. DOI: 10.1038/msb.2010.56.
- [23] K. Jungermann and N. Katz. “Functional specialization of different hepatocyte populations”. In: *Physiological reviews* 69.3 (1989), pp. 708–764. ISSN: 0031-9333. DOI: 10.1152/physrev.1989.69.3.708.
- [24] L. Kaderali et al. “CASPAR: a hierarchical Bayesian approach to predict survival times in cancer from gene expression data”. In: *Bioinformatics* 22.12 (2006), pp. 1495–1502.
- [25] M. König, S. Bulik, and H.-G. Holzhütter. “Quantifying the contribution of the liver to glucose homeostasis: a detailed kinetic model of human hepatic glucose metabolism.” In: *PLoS computational biology* 8 (6 2012), e1002577. ISSN: 1553-7358. DOI: 10.1371/journal.pcbi.1002577.
- [26] M. König and H.-G. Holzhütter. “Kinetic modeling of human hepatic glucose metabolism in type 2 diabetes mellitus predicts higher risk of hypoglycemic events in rigorous insulin therapy.” In: *The Journal of biological chemistry* 287 (44 Oct. 2012), pp. 36978–36989. ISSN: 1083-351X. DOI: 10.1074/jbc.M112.382069.

- [27] Y. Kogan et al. “A new validated mathematical model of the Wnt signalling pathway predicts effective combinational therapy by sFRP and Dkk”. In: *The Biochemical journal* 444.1 (2012), pp. 115–125. ISSN: 0264-6021. DOI: 10.1042/BJ20111887.
- [28] M. König. *Executable Simulation Model of the Liver*. Vol. 2. 2020. DOI: 10.1101/2020.01.04.894873.
- [29] T. Köppl, E. Vidotto, and B. Wohlmuth. “A 3D-1D coupled blood flow and oxygen transport model to generate microvascular networks”. In: *International Journal for Numerical Methods in Biomedical Engineering* (2020), e3386. ISSN: 2040-7947. DOI: \url{10.1002/cnm.3386}.
- [30] A. Kramer, B. Calderhead, and N. Radde. “Hamiltonian Monte Carlo methods for efficient parameter estimation in steady state dynamical systems”. In: *BMC bioinformatics* 15 (2014), p. 253. DOI: 10.1186/1471-2105-15-253.
- [31] C. Kreutz et al. “Profile likelihood in systems biology”. In: *FEBS J* 280 (2013), pp. 2564–2571. DOI: 10.1111/febs.12276.
- [32] S. Krishan et al. “Non-invasive quantification of hepatic steatosis in living, related liver donors using dual-echo Dixon imaging and single-voxel proton spectroscopy”. en. In: *Clin Radiol* 71.1 (Jan. 2016), pp. 58–63. ISSN: 00099260. DOI: 10.1016/j.crad.2015.10.002. URL: <https://linkinghub.elsevier.com/retrieve/pii/S000992601500389X> (visited on 01/24/2020).
- [33] P. Kügler, E. Gaubitzter, and S. Müller. “Parameter identification for chemical reaction systems using sparsity enforcing regularization: A case study for the chlorite-Iodide reaction”. In: *J. Phys. Chem.* 113.12 (2009), pp. 2775–2785.
- [34] L. Lambers, T. Ricken, and M. König. “Model Order Reduction (MOR) of Function-Perfusion-Growth Simulation in the Human Fatty Liver via Artificial Neural Network (ANN)”. In: *PAMM* 19.1 (2019), e201900429. DOI: 10.1002/pamm.201900429. eprint: <https://onlinelibrary.wiley.com/doi/pdf/10.1002/pamm.201900429>. URL: <https://onlinelibrary.wiley.com/doi/abs/10.1002/pamm.201900429>.
- [35] L. Lambers, N. Waschinsky, and T. Ricken. “On a Multi-Scale and Multi-Phase Model of Paracetamol-induced Hepatotoxicity for Human Liver”. In: *PAMM* 18.1 (2018), e201800454. ISSN: 1617-7061. DOI: 10.1002/pamm.201800454.
- [36] P. Martirosian et al. “Spatial-temporal perfusion patterns of the human liver assessed by pseudo-continuous arterial spin labeling MRI”. en. In: *Z Med Phys* 29.2 (May 2019), pp. 173–183. ISSN: 09393889. DOI: 10.1016/j.zemedi.2018.08.004. URL: <https://linkinghub.elsevier.com/retrieve/pii/S0939388918300618> (visited on 01/27/2020).
- [37] A. Mielke and T. Ricken. “Evaluating Artificial Neural Networks and Quantum Computing for Mechanics”. In: *PAMM* 19.1 (2019).
- [38] A. Naik, D. Rozman, and A. Belič. “SteatoNet: the first integrated human metabolic model with multi-layered regulation to investigate liver-associated pathologies”. In: *PLoS Computational Biology* 10 (12 Dec. 2014), e1003993. ISSN: 1553-7358. DOI: 10.1371/journal.pcbi.1003993.
- [39] N. A. O’Leary et al. “Reference sequence (RefSeq) database at NCBI: current status, taxonomic expansion, and functional annotation”. In: *Nucleic acids research* 44.D1 (2016), pp. D733–D745.
- [40] J. D. Orth, I. Thiele, and B. Ø. Palsson. “What is flux balance analysis?” In: *Nature biotechnology* 28.3 (2010), pp. 245–248. DOI: 10.1038/nbt.1614.
- [41] R. Pagliarini et al. “In Silico Modeling of Liver Metabolism in a Human Disease Reveals a Key Enzyme for Histidine and Histamine Homeostasis.” In: *Cell reports* 15 (10 June 2016), pp. 2292–2300. ISSN: 2211-1247. DOI: 10.1016/j.celrep.2016.05.014.
- [42] M. Pertea et al. “CHESS: a new human gene catalog curated from thousands of large-scale RNA sequencing experiments reveals extensive transcriptional noise”. In: *Genome biology* 19.1 (2018), pp. 1–14.
- [43] D. M. Pierce, T. Ricken, and G. A. Holzapfel. “Modeling sample/patient-specific structural and diffusional responses of cartilage using DT-MRI”. In: *International Journal for Numerical Methods in Biomedical Engineering* 29.8 (2013), pp. 807–821. ISSN: 2040-7947.
- [44] Y. Qin et al. “Determination of liver volume in vivo in rats using MRI”. en. In: *Eur J Radiol* 11.3 (Nov. 1990), pp. 191–195. ISSN: 0720048X. DOI: 10.1016/0720-048X(90)90054-F. URL: <https://linkinghub.elsevier.com/retrieve/pii/0720048X9090054F> (visited on 01/24/2020).
- [45] N. Radde and J. Offtermatt. “Convergence of posteriors for structurally non-identifiable problems using results from the theory of inverse problems”. In: *J Inverse Ill-Posed P* 22.2 (2013), pp. 251–76. DOI: 10.1515/jip-2012-0057.
- [46] R. Ramasawmy et al. “Hepatic arterial spin labelling MRI: an initial evaluation in mice”. en. In: *NMR Biomed.* 28.2 (Feb. 2015), pp. 272–280. ISSN: 09523480. DOI: 10.1002/nbm.3251. URL: <http://doi.wiley.com/10.1002/nbm.3251> (visited on 01/27/2020).
- [47] A. Raue et al. “Comparison of approaches for parameter identifiability analysis of biological systems”. In: *Bioinformatics* 30.10 (2014), pp. 1440–1448. DOI: 10.1093/bioinformatics/btu006.

- [48] A. Raue et al. “Structural and practical identifiability analysis of partially observed dynamical models by exploiting the profile likelihood”. In: *Bioinformatics* 25.15 (2009), pp. 1923–1929.
- [49] D. Reddyhoff et al. “Timescale analysis of a mathematical model of acetaminophen metabolism and toxicity.” In: *Journal of theoretical biology* 386 (Dec. 2015), pp. 132–146. ISSN: 1095-8541. DOI: 10.1016/j.jtbi.2015.08.021.
- [50] T. Ricken and L. Lambers. “On computational approaches of liver lobule function and perfusion simulation”. In: *GAMM-Mitteilungen* 9.3 (2019), e201900016. ISSN: 0936-7195. DOI: 10.1002/gamm.201900016.
- [51] T. Ricken, N. Waschinsky, and D. Werner. “Simulation of Steatosis Zonation in Liver Lobule—A Continuum Mechanical Bi-Scale, Tri-Phasic, Multi-Component Approach”. In: *Biomedical Technology*. Ed. by P. Wriggers and T. Lenarz. Vol. 84. Lecture Notes in Applied and Computational Mechanics. Cham: Springer International Publishing, 2018, pp. 15–33. ISBN: 978-3-319-59547-4. DOI: 10.1007/978-3-319-59548-1_2.
- [52] T. Ricken et al. “Concentration driven phase transitions in multiphase porous media with application to methane oxidation in landfill cover layers”. In: *ZAMM-Journal of Applied Mathematics and Mechanics/Zeitschrift für Angewandte Mathematik und Mechanik* 94.7 (2014), pp. 609–622.
- [53] T. Ricken et al. “Modeling function-perfusion behavior in liver lobules including tissue, blood, glucose, lactate and glycogen by use of a coupled two-scale PDE-ODE approach.” In: *Biomechanics and Modeling in Mechanobiology* 14 (3 June 2015), pp. 515–536. ISSN: 1617-7940. DOI: 10.1007/s10237-014-0619-z.
- [54] E. K. Rodriguez, A. Hoger, and A. D. McCulloch. “Stress-dependent finite growth in soft elastic tissues”. In: *Journal of Biomechanics* 27 (4) (1994), pp. 455–467. ISSN: 0021-9290.
- [55] S. Roy et al. “A general overview on non-coding RNA-based diagnostic and therapeutic approaches for liver diseases”. In: *Frontiers in pharmacology* 9 (2018), p. 805.
- [56] J. Schleicher et al. “A theoretical study of lipid accumulation in the liver—implications for non-alcoholic fatty liver disease.” In: *Biochimica et Biophysica Acta* 1841 (1 Jan. 2014), pp. 62–69. ISSN: 0006-3002. DOI: 10.1016/j.bbapap.2013.08.016.
- [57] J. Schleicher et al. “Zonation of hepatic fat accumulation: insights from mathematical modelling of nutrient gradients and fatty acid uptake.” In: *Journal of the Royal Society, Interface* 14 (133 Aug. 2017). ISSN: 1742-5662. DOI: 10.1098/rsif.2017.0443.
- [58] L. O. Schwen et al. “Algorithmically generated rodent hepatic vascular trees in arbitrary detail”. In: *Journal of Theoretical Biology* 365.0 (2015), pp. 289–300. ISSN: 0022-5193. DOI: \url{10.1016/j.jtbi.2014.10.026}.
- [59] C. H. Thng. “Perfusion magnetic resonance imaging of the liver”. en. In: *World J Gastroenterol* 16.13 (2010), p. 1598. ISSN: 1007-9327. DOI: 10.3748/wjg.v16.i13.1598. URL: <http://www.wjgnet.com/1007-9327/full/v16/i13/1598.htm> (visited on 01/24/2020).
- [60] B. Verma, P. Subramaniam, and R. Vadigepalli. “Model-based virtual patient analysis of human liver regeneration predicts critical perioperative factors controlling the dynamic mode of response to resection”. In: *BMC Syst Biol* 13.9 (2019). DOI: 10.1186/s12918-019-0678-y.
- [61] D. Werner. *Two Scale Multi-component and Multi-phase Model for the Numerical Simulation of Growth Processes in Saturated Porous Media under Consideration of Bio-chemical Processes - at the Example of the Human Liver*. 1. Auflage. Berichte aus der Biomechanik. Aachen: Shaker, 2017. ISBN: 3844054626.
- [62] A. Woller et al. “A Mathematical Model of the Liver Circadian Clock Linking Feeding and Fasting Cycles to Clock Function”. In: *Cell reports* 17.4 (2016), pp. 1087–1097. DOI: 10.1016/j.celrep.2016.09.060.

Simulating Clinically Relevant Cases in Cardiology via Numerical Tools

by Barış Cansız, Yongjae Lee, Lucas A. Woodworth & Michael Kaliske

Institute for Structural Analysis, Technische Universität Dresden, Germany

1 Introduction

The initial beat of the human heart occurs in the early stages of embryo development and continues ceaselessly until death of the body. The heart is the core unit of the cardiovascular system whose task is to sustain a continuous blood circulation throughout the body, thereby nourishing every single cell with essential substrates, enabling waste excretion and keeping the whole system functioning under various conditions (e.g. resting, training, pregnancy). Hence, any dysfunction in the circulation system might lead to critical conditions such as loss of standard of living, stroke or even sudden death. According to the World Health Organization, 17.9 million people die from cardiovascular diseases (CVDs) in the world each year, which corresponds to 31% of all global deaths. Apart from deep impact on human life, CVDs cause high a financial burden for the society resulting from direct costs, e.g. medical care, and indirect costs, e.g. labour force loss, which was estimated around \$ 555 billion in 2015 in the United States. Unfortunately, mortality and economical side effects of CVDs are projected to increase over the next 20 years [2].

These harsh facts canalized scientists to understand how a healthy heart functions and how heart diseases progress with the aim to achieve robust diagnostic tools and efficient treatment strategies. A huge amount of research groups perform clinical experiments and trials on humans and animals in order to deepen our understanding of the heart and how CVDs develop. Undoubtedly, such studies greatly benefit the field of cardiology. However, the requirement of high budgets, long follow-up durations, trial and error procedures and ethic approvals limit the progress [9, 15]. In addition, the reproducibility and generalization of experimental findings are another critical issue. On the clinical side, one is able to assess the current status of a patient's cardiac function through non-invasive techniques, e.g. computer tomography (CT), cardiac magneto resonance imaging (cMRI), echocardiography (echo), electrocardiogram (ECG), and invasive techniques, e.g. blood tests, biopsy, catheterization. However, these diagnostic tools cannot provide a complete understanding of the cardiac function and possible disease progression. One of the demanding issues is the existence of unique properties and conditions of each patient's heart that makes it difficult to establish a general consensus on diagnosis, possible disease progression and treatment methodology.

On the other hand, it is a well known fact that the recognition of a disease and its treatment technique for a specific patient are deduced in the light of a physiologist's experience that is naturally subjective to a certain extent and does

not necessarily guarantee the best outcome. It is speculated that a large number of people are subjected to misdiagnosis, causing serious health problems, deaths and additional costs that could have been prevented [12]. Therefore, more efficient diagnostic approaches pinpointing the cause of disease and precise patient-specific treatment strategies are extremely desirable in order to reduce the mortality and economical side effects of heart diseases.

In this context, computing facilities along with advancements in numerical modelling approaches for the heart provide a promising investigation opportunity. Thanks to numerical developments, it will be feasible to virtually analyze a patient's heart, predict possible disease progression patterns and provide information that is not possible to obtain through medical monitoring tools alone, e.g. stress distribution in the intact ventricle. It would be no surprise if the near future would witness cardiologists who are educated with basic engineering knowledge and performing predictive patient-specific simulations as a clinical routine before making a final decision on a treatment methodology. Nevertheless, computational modelling of such a complex organ is not a straightforward task since various constituents (electrophysiology, contraction, boundary conditions, blood flow, valves etc.), which regulate heart function, have to be considered.

In this contribution, we briefly introduce some important aspects of our recently established finite element (FE)-based numerical framework in the context of computational modelling of the heart. Furthermore, we present some elaborate numerical examples which demonstrate the usability of our numerical framework for cases encountered in cardiology departments of hospitals.

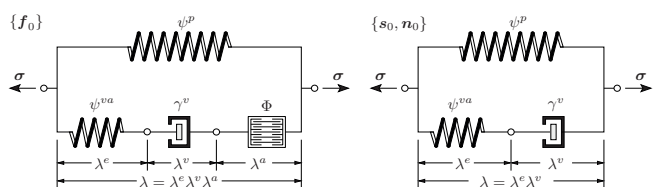


Figure 1: Rheology for the electro-visco-elastic response of the myocardium.

2 Excitation and contraction coupling in myocardial tissue

The electromechanical state of the heart muscle, or in other words, the myocardium is governed by the balance of linear momentum and a reaction-diffusion-type equation of excitation either in the monodomain [10] or bidomain setting [7, 8], depending on the nature of the problem. The coupling between the mechanical and electrical fields is established through relations at the constitutive level.

In order to achieve an extensive description of the active myocardial behaviour, we developed a sophisticated rheology considering orthotropic electro-visco-elastic aspects of the myocardium. As a first step in the development of the model, the myocardium is deemed as a passive material and a rheological model that consists of two branches connected in parallel is considered. One branch is related to the equilibrium response through an elastic spring and the other branch represents the non-equilibrium response through a spring+dashpot element. Regarding the orthotropic viscous properties of the myocardial tissue, the non-equilibrium part of the free energy function is additively decomposed into fibre, sheet and normal directions and each orientation is associated with distinct material parameters [6]. Furthermore, this rheology is furnished with a contractile element only along the fibre direction in order to describe the active tissue response, i.e. the influence of the electrical excitation on the mechanical field, while the material response along the sheet and normal directions is assumed to be passive. The resulting setting can be considered as an extension of the classical Hill model [13] to account for the viscosity in the three-dimensional space which we name as the modified Hill model [3], see Figure 1.

The model considers the multiplicative decomposition of the total deformation gradient into an elastic part \mathbf{F}^e , a viscous part \mathbf{F}^v and an active part \mathbf{F}^a

$$\mathbf{F} = \mathbf{F}^e \mathbf{F}^v \mathbf{F}^a. \quad (1)$$

The viscous part of the deformation gradient embodies the orthotropic viscous properties and the active part of the deformation gradient manifests the contractile nature of the heart tissue. Both of the sub-parts are prescribed according to the orthotropic properties of the myocardium

$$\begin{aligned} \mathbf{F}^v &:= \mathbf{1} + (\lambda_f^v - 1) \mathbf{f}_0 \otimes \mathbf{f}_0 \\ &\quad + (\lambda_s^v - 1) \mathbf{s}_0 \otimes \mathbf{s}_0 + (\lambda_n^v - 1) \mathbf{n}_0 \otimes \mathbf{n}_0, \end{aligned} \quad (2)$$

$$\mathbf{F}^a := \mathbf{1} + (\lambda_f^a - 1) \mathbf{f}_0 \otimes \mathbf{f}_0.$$

Herein, the viscous stretches λ_f^v , λ_s^v and λ_n^v and the active stretch λ_f^a are associated with the fibre \mathbf{f}_0 , sheet \mathbf{s}_0 and normal \mathbf{n}_0 directions that are assumed to be perpendicular to each other in the reference state. This assumption further leads to a multiplicative decomposition of the stretches without any coupling between the directions $\lambda_f = \lambda_f^e \lambda_f^v \lambda_f^a$, $\lambda_s = \lambda_s^e \lambda_s^v$ and $\lambda_n = \lambda_n^e \lambda_n^v$, where the superscript e designates the elastic part of the stretch. The viscous stretches represent the deformation

in the dashpot along three orthogonal directions governed by the macroscopic deformation, while the active stretch represents the shortening of the myocardium along the fibre direction emerging from an alteration in the intracellular calcium concentration which is formulated in terms of the transmembrane potential. Both stretches as well as the intracellular calcium concentration are considered as internal variables in the framework.

After determining the viscous and active parts of the stretches, the elastic part of the deformation gradient can be simply obtained through relation $\mathbf{F}^e = \mathbf{F}(\mathbf{F}^v \mathbf{F}^a)^{-1}$. Moreover, in line with the rheological setting, the total free energy function is additively decomposed into passive $\hat{\psi}^p$ and visco-active $\hat{\psi}^{va}$ parts

$$\psi(\mathbf{s}; \mathbf{F}, \mathbf{F}^e) = \hat{\psi}^p(\mathbf{s}; \mathbf{F}) + \hat{\psi}^{va}(\mathbf{s}; \mathbf{F}^e) \quad (3)$$

with $\mathbf{s} = \{\mathbf{f}_0, \mathbf{s}_0, \mathbf{n}_0\}$. Note that this setting comprises the advantages of both the additive split of the total stress and the multiplicative decomposition of the total deformation gradient in the sense of Göktepe et al. [11].

When it comes to the modelling of cardiac electrophysiology at the material level, two essential approaches can be mentioned: ionic and phenomenological models. The ionic models represent a sophisticated description of the cardiomyocytes by considering the local evolution of individual ion species in line with experimental observations, e.g. Ten Tusscher-Noble-Noble-Panfilov model [17]. These models are useful when one needs to study the influence of a particular ion activity on cardiac electrophysiology, e.g. drug application. However, a high number of evolution equations for ion concentrations, ionic currents and gating variables requires a demanding computational treatment. On the other hand, for the investigation of electrical wave propagation in healthy and pathological cases (e.g. arrhythmia, dyssynchrony) on the tissue or organ level, the phenomenological models are convenient due to their easiness of implementation and relatively reduced computational effort compared to the ionic models. In this context, the Aliev-Panfilov model [1] is one of most employed approaches which provides an excellent description of myocyte excitation. The model is able to mimic the intrinsic characteristics of the transmembrane potential and lumps the influence of all ionic currents in a single slow recovery variable. Within this contribution, both of the aforementioned models are employed.

Moreover, a mechanical deformation causing a myocardial elongation can induce an additional ion transmission through the membrane that might alter the electrical activity of the myocardium and this phenomenon is called mechano-electric feedback (MEF). MEF is often described by a simple equation that is a linear function of the stretch along the fibre direction in accordance with the experimental observations [16].

3 Application of the numerical framework to real-life situations

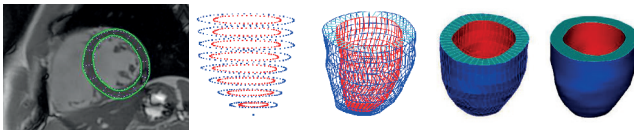


Figure 2: Generation of a virtual biventricular model from cMRI data. From left to right, segmentation of the left ventricle (LV) endocardial and epicardial wall at end-diastole on one of the slices in the short axis view, construction of the frame through the coordinates obtained from the segmentation, creation of truss elements over the boundaries, creation of surface elements over the boundaries and creation of 3D solid by unifying all surface elements on the boundary. The right ventricle is generated by following the same steps and is then unified with the LV to obtain the virtual biventricular heart model.

3.1 Fibrillation and defibrillation

One of the important pathologies encountered in cardiology departments is rhythm disorders, e.g., fibrillation, bradycardia and tachycardia. Among them, ventricular fibrillation necessitates an urgent intervention since the heart cannot pump blood anymore and death or permanent damage can occur in a couple of minutes. Applying an external electrical field, which is often called defibrillation, is a frequently utilized effective technique to terminate the chaotic electrical activity. The aim is to constitute an electric circuit in the cardiac tissue through which the currents propagate and to bring the chaotic electrical activity to an end.

In the following, an FE simulation of a virtualized biventricular heart model is demonstrated where regular beat, arrhythmia and recovery of the regular beat by applying an external shock are mimicked. Moreover, an ECG is recorded during the entire simulation which is one of the most frequently utilized diagnostic tools, since it can be non-invasively and immediately obtained and guide cardiologists to reveal the abnormalities in electrical activity and contraction of the heart. The virtual biventricular heart model is generated from a cMRI of a 38-year old healthy volunteer's (male) biventrices, see Figure 2. In the simulation, the mechanical field is not considered. The interested reader is referred to [4] for a more extensive (de)fibrillation example including the mechanical field.

The snapshots belonging to the numerical analysis are demonstrated in Figure 3 along with the graph depicting the ECG. The excitation of the ventricles is initiated with depolarization of the atrioventricular node and the first regular cardiac cycle is presumed to start at time $t = 100$ ms. In the following

cycle beginning at time $t = 900$ ms, after the ventricles start to go through the repolarization phase, an arrhythmia is induced by injecting an extra current to the material points that stand in the tail of the repolarizing wave, see the snapshot at time $t = 1314$ ms. The applied external stimulus also reveals itself on the T-wave segment in the ECG, where the ventricles are vulnerable to an arrhythmia. After destroying the regular heart rhythm, a clear manifestation of the reentrant scroll wave is present in the snapshots. On the other hand, disordered deflections are observed with changing magnitude and formation in the ECG, which also indicates a fibrillatory state of the ventricles. In clinical routine, such a diagnosis would be swiftly treated by applying an external shock.

In order to mimic this phenomenon, an electrical field is generated by applying an outflux and an influx to a small region on the LV epicardium and the LV endocardium, respectively, in the time interval $t \in [3410, 3460]$. Upon the applied shock, the chaotic electrical wave propagation, i.e. arrhythmia, is terminated and the ventricles go into a completely repolarized state. Thereafter, the ventricles are again depolarized from the atrioventricular node at time $t = 4100$ ms. Observe that an inverse T-wave in the ECG, indicating an abnormal transmembrane potential distribution, is displayed in the cycle right after the defibrillation. This electrical irregularity undoubtedly arises from the perturbed restitution properties of the myocardium during the arrhythmia. However, the restitution properties and usual transmembrane potential distribution are recovered and the ECG takes its regular shape as the ventricles are further excited.

3.2 Cardiac resynchronization therapy

Another serious pathological condition of the heart is ventricular dyssynchrony which occurs most likely due to abnormal electrical conduction. For example, left or right bundle branch block, scar tissue, infarcted regions or cardiomyopathy might result in irregular electrical wave propagation leading to unsynchronized mechanical activations, unusual loading conditions and deformations of the myocardium. In most cases, the result is unfortunately heart failure. This pathology is often manifested as a long QRS duration (> 130 ms) in ECG and a considerably diminished LV ejection fraction (EF). In such cases, cardiac resynchronization therapy (CRT) is one of the most frequently used treatment methodologies for patients having reduced cardiac pump function.

The idea behind CRT is to deliver electrical pulses to specific regions in the heart, thereby synchronizing the contraction and increasing the cardiac output. In this example, we mimic CRT in the virtualized biventricle model and demonstrate how we improve the cardiac function by applying external electrical pulses in computer simulation. In the simulation, both electrical and mechanical fields are considered.

In the model, dyssynchrony is induced by altering the ma-

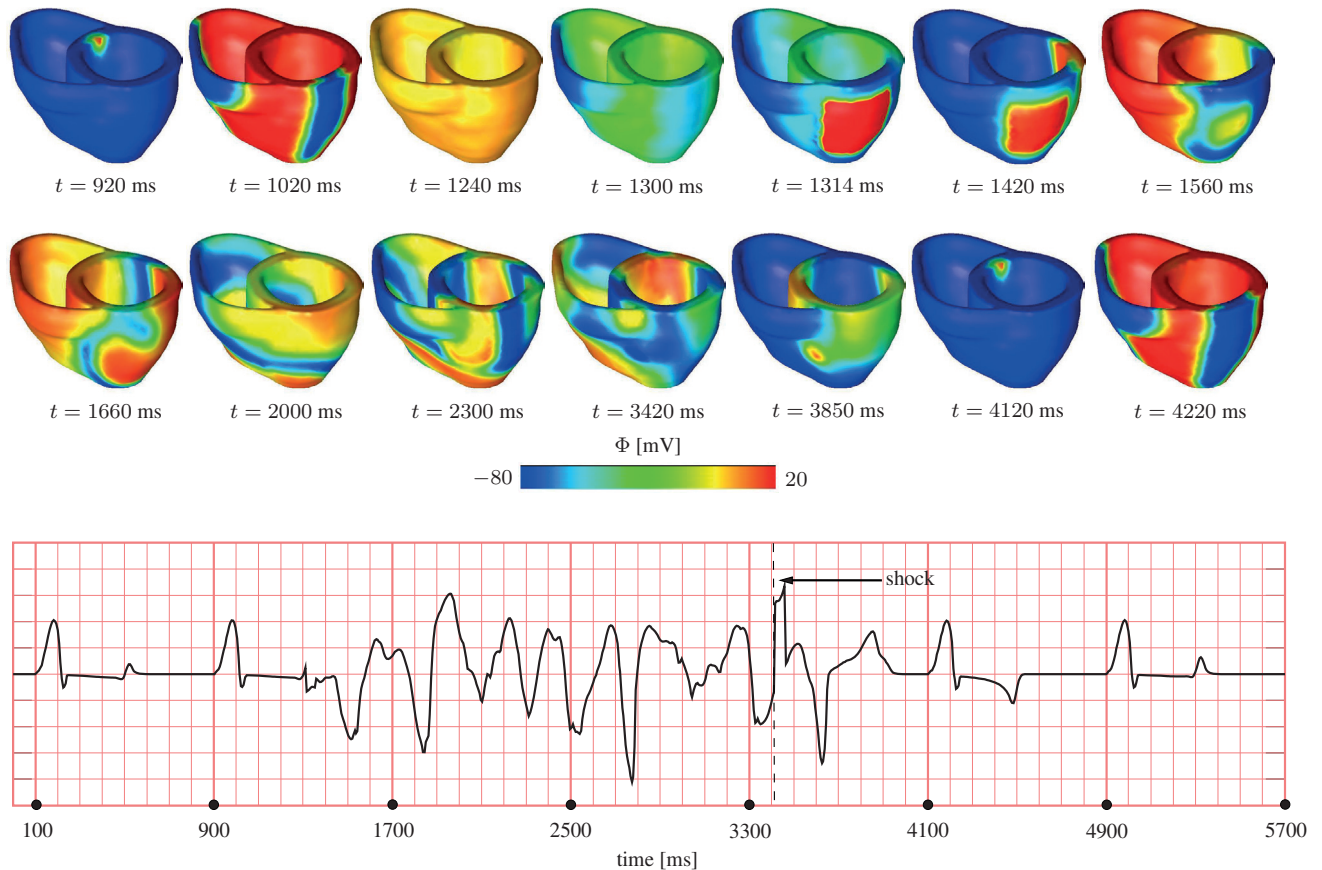


Figure 3: Demonstration of regular heart beat, arrhythmia and its termination (defibrillation) by an externally applied electrical field. In the snapshots, the transmembrane potential distribution is shown and the graph presents the ECG, normalized voltage, recorded during the simulation.

terial parameters throughout some regions of the biventricle, shown in Figure 4, so that the tissue becomes more stiff, the contractility is diminished, the action potential duration is increased and the conduction velocity is considerably reduced. Hence, this region turns into an obstacle for the propagating electrical waves and contracts weakly. The result is a dysfunction of the ventricles, which is indicated by the prolonged QRS complex (144 ms) in the ECG and the low LV EF (29 %) in the volume-time (v-t) diagram, see the first two cycles in Figure 5. In order to improve the cardiac output, we start applying the CRT with the cycle beginning at time $t = 1700$ ms throughout three subsequent cycles in terms of an outflux to a small region on the endocardial surface of the right ventricle and an influx to a small region on the epicardial surface of the LV free wall, see Figure 4 (right) for the pacing sites. Upon the CRT, we achieve notable improvements in the cardiac function. The QRS complex is shortened to 122 ms and an elevation of 17 ml in SV and 9% in EF of the LV is observed, which could be considered a desirable improvement of cardiac systolic function in clinical routine. Note that upon the application of the CRT, a significantly different morphology in the ECG appears due to the altered pattern of electrical wave propagation. For instance, as the depolarization wave front propagates from the base to the apex, it suddenly changes its orientation for a short time to the opposite direction, which is displayed as a zigzag in the QRS complex. In addition, we observe a smaller T-wave amplitude implying a slower repolarization process of the ventricles due to the altered restitution properties. At the end, we stop applying the external electrical field after three cardiac cycles and beginning from time $t = 4100$ ms, the ECG morphology and LV v-t relation turn back to their initial values as those before the CRT is applied. A more detailed discussion of CRT simulation and its comparison to the healthy case can be found in [5].

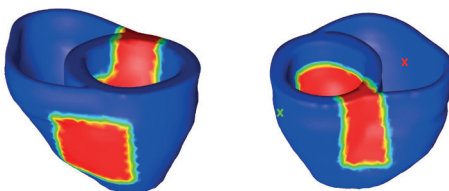


Figure 4: Illustration of the infarcted zone from different views and the pacing sites during the CRT attempts. The regions in red colour are infarcted while the healthy regions have blue colour. In the second view (right), the green and red crosses depict the influx and outflux sites, respectively, during the CRT.

3.3 Commotio cordis and precordial thump

Though rare, one can experience a life-threatening arrhythmia leading to sudden cardiac death although there is no sign of cardiac disease [14]. This event can simply originate from a

moderate impact to the chest which causes an abnormal deformation of the heart. The result is the generation of unexpected electrical stimuli through stretch-activated ion-channels (i.e. MEF) which disturb the regular rhythm of the heart. This phenomenon is mostly seen in young athletes playing e.g. baseball or ice hokey, where there is a high risk of an impact to the chest. In case of such an arrhythmia, an immediate application of a defibrillator device increases the chance of survival. However, in the absence of a defibrillator, a moderate impact to the chest, which is known as precordial thump, might be an effective intervention to terminate the irregular heart rhythm.

These phenomena are mimicked with our numerical framework in the biventricle model and the results are presented in Figure 6. The regular excitation-contraction coupling is disturbed by a blunt impact to the precordial LV region, noted as 1st impact in the ECG. Observe that the mechanical impact is applied within the time period where the ventricles are vulnerable to arrhythmia, as done in the first example in which we induce arrhythmia via external stimuli. Thereafter, the ECG indicates a chaotic wave propagation in the ventricles. Consequently, the heart cannot pump blood as manifested in the LV v-t diagram. Nearly 3.7 seconds after the beginning of the arrhythmia, we apply a second mechanical impact, noted as 2nd impact in the ECG, causing stretch activated ion-channels to generate another electrical stimulus which eventually becomes an obstacle for the arrhythmia and terminates it.

3.4 Application of a drug: verapamil

In this example, we demonstrate the application of a drug called verapamil which is known as a calcium channel blocker. Verapamil is often used to treat patients having hypertension, high ventricular rate and chest pain. It takes effect by blocking certain ion channels on the cell membrane, which leads to reducing the muscle contractility as a result of diminished intracellular calcium concentration, so that blood vessels are dilated and the load on the heart is lowered. Accordingly, the heart relaxes and does not have to pump the blood so strongly.

In order to study the effect of verapamil on the electromechanical behaviour of the ventricles, we consider a control case and two drug cases with different concentrations of verapamil. Different from the previous examples, the cardiac electrophysiology is described by the ionic model of ten Tusscher et al. [17] and a personalized LV model from echo is used in the simulations, see Figure 7. The results of the simulations are presented in terms of an ECG and a v-t relation for each case in Figure 8.

The control simulation displays a regular ECG with a satisfactory duration of the QRS and QT intervals. Moreover, an EF of 69 % is measured. These markers indicate a physiological range for the electrophysiology and the mechanics of the LV behaviour. On the other hand, when a verapamil con-

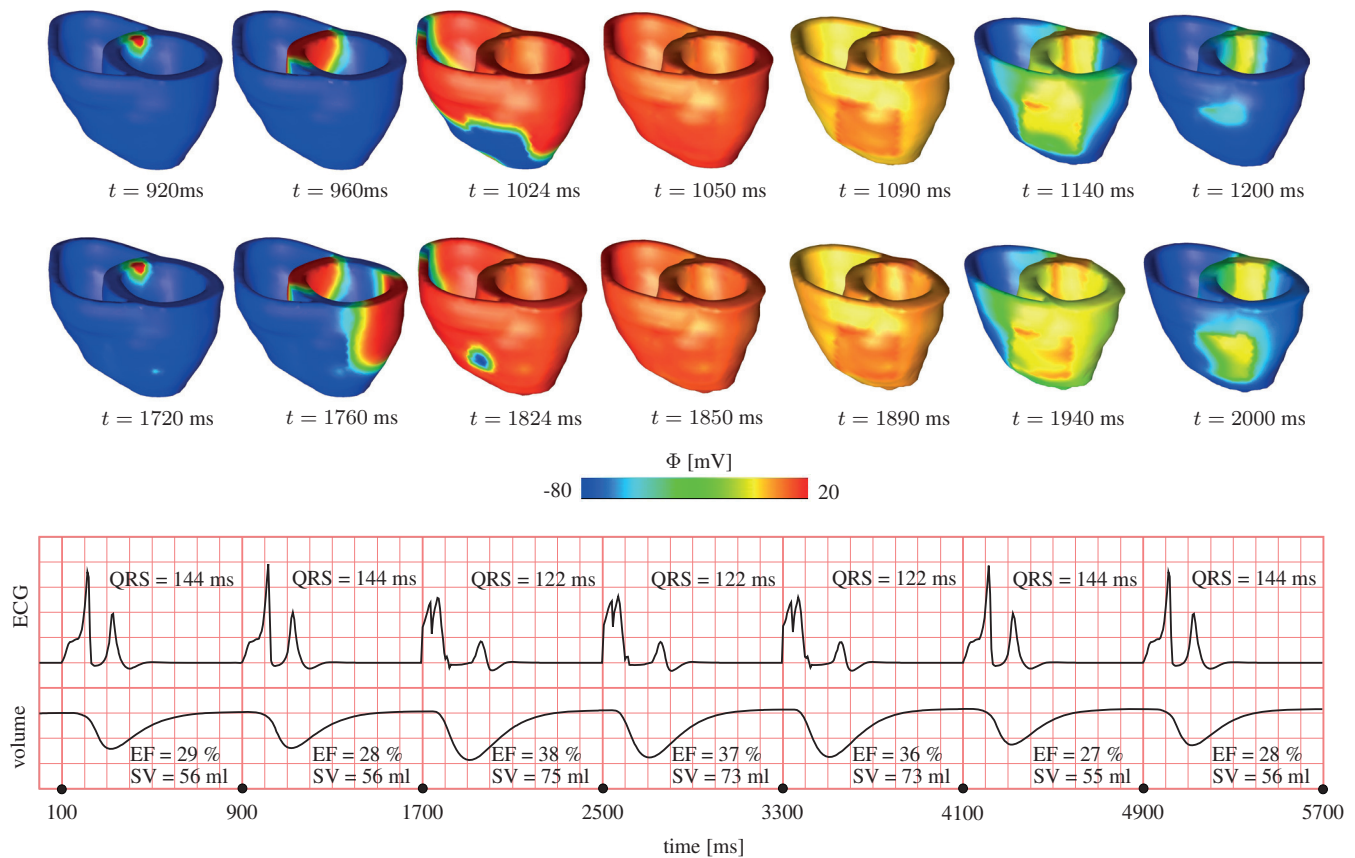


Figure 5: Demonstration of cardiac cycles without and with CRT in the dyssynchronous model. In the snapshots, the transmembrane potential distribution is shown and the graph presents the ECG, normalized voltage (upper curve), and LV v-t diagram, normalized volume (lower curve), recorded during the simulation. Moreover, the QRS duration, stroke volume (SV) and EF are given for each cycle.

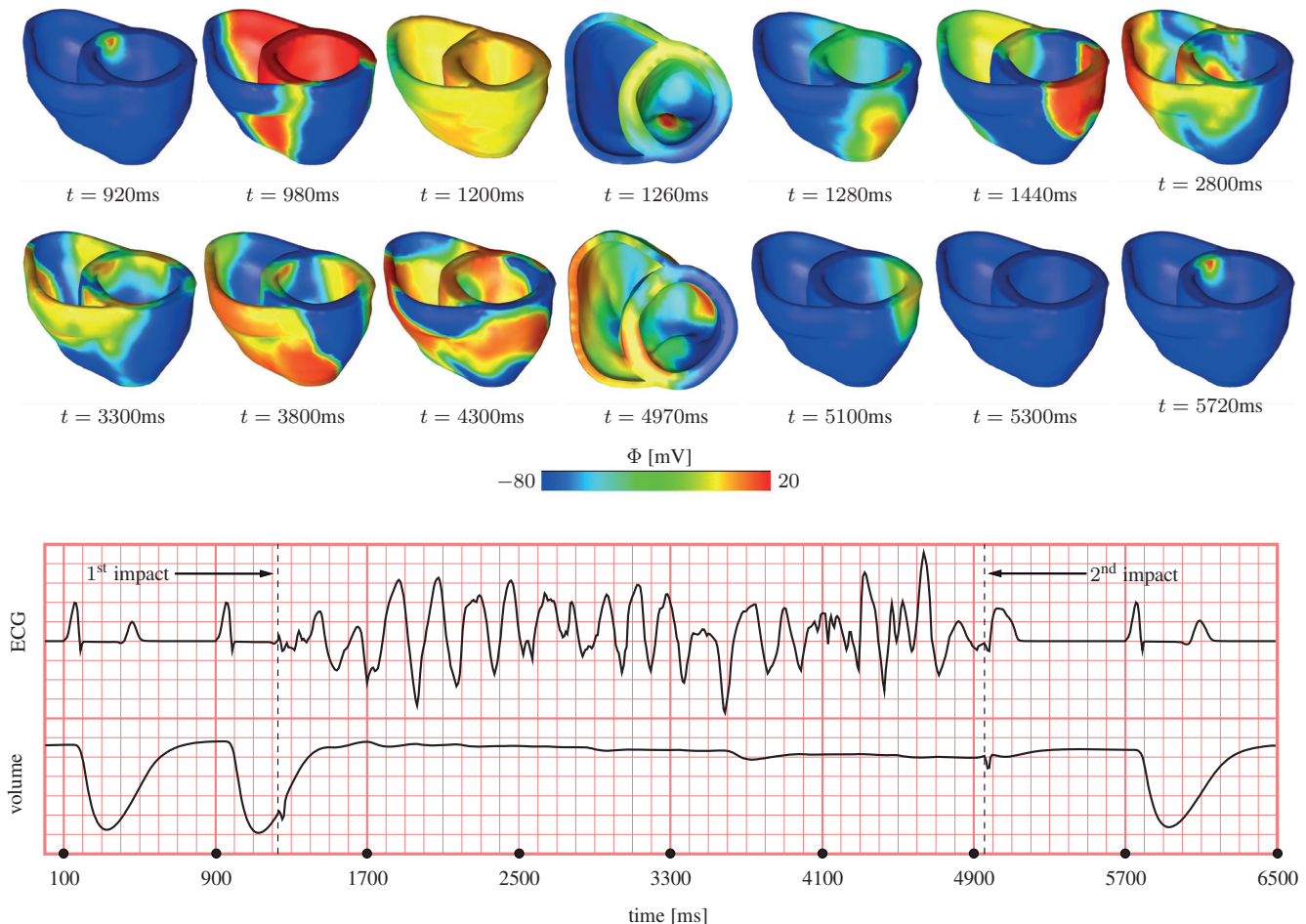


Figure 6: Demonstration of commotio cordis and precordial thump. In the snapshots, the transmembrane potential distribution is shown and the graph presents the ECG, normalized voltage, and LV v-t diagram, normalized volume (lower curve), recorded during the simulation. Note that the snapshots at time $t = 1260$ ms and $t = 4970$ ms are taken at different views in order to make the mechanical impact more visible.

centration of 100 nM is applied, repolarization occurs earlier and more uniformly causing a smaller QT interval and a reduction in the magnitude of the T-wave. Besides, verapamil suppresses the contractility, i.e. the active stretch, leading to a reduced EF of 58 % and a decrease in the duration of ventricular contraction (systole).

Furthermore, the larger concentration of verapamil with 1500 nM makes the repolarization and end-systole occur much earlier. The QT interval decreases significantly and the T-wave is inverted. In addition, a low EF of 35 % is obtained along with a much reduced systole duration. Furthermore, the duration of the QRS complex remains constant, while its magnitude decreases for higher concentrations of verapamil. The tendency observed in the ECGs and v-t relations can be explained as follows. The action potential duration of myocytes is reduced as the concentration of verapamil is increased. This causes an abbreviated QT interval and also affects the action potential duration dispersion leading to the smaller and inverted T-wave. Additionally, verapamil lowers the magnitude of the active stretch, resulting in a smaller EF.

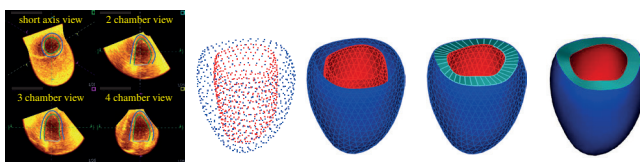


Figure 7: The steps of the virtual LV model generation from 4D echo data. From left to right, segmentation of the endocardial and epicardial surfaces at end-diastole, construction of the endocardial and epicardial frame through the coordinates obtained from the segmentation, creation of surface elements over the endocardium and epicardium, creation of surface elements over the basal region in order to obtain a closed volume and unification of all surface elements in order to create a solid LV geometry.

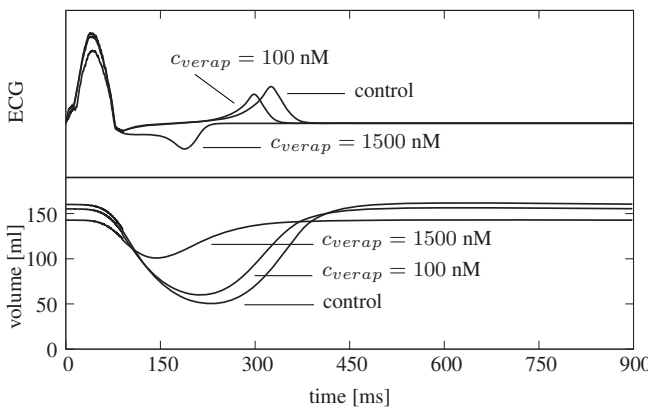


Figure 8: Illustration of the application of two concentrations of verapamil ($c_{verap} = 100$ and 1500 nM) and its comparison to the control case ($c_{verap} = 0$ nM). The graph presents the ECG, normalized voltage, (upper curves) and v-t diagram (lower curves).

4 Conclusion

The advent of computational facilities provides a great possibility for examining the heart in a virtual manner, i.e. non-invasive, cheap and fast. In the near future, cardiologists will undoubtedly derive more and more benefits from numerical tools for gaining deep insight into the working mechanisms of the heart and developing successful patient-specific treatment methods. In this contribution, we presented our latest numerical developments serving as a milestone towards this ultimate goal. We illustrated the feasibility of the numerical scheme through elaborate numerical examples that are clinically relevant and interesting.

Acknowledgement

We gratefully acknowledge the contribution of Dr. med. Krunoslav Michael Sveric and Prof. Dr. med. Axel Linke from Department of Cardiology, Heart Center, Technische Universität Dresden and the financial support of the German Research Foundation (DFG) under grants KA 1163/18 and KA 1163/49.

References

- [1] R. R. Aliev and A. V. Panfilov. A simple two-variable model of cardiac excitation. *Chaos, Solitons & Fractals*, 7:293–301, 1996.
- [2] E. J. Benjamin, P. Muntner, A. Alonso, M. S. Bittencourt, C. W. Callaway, A. P. Carson, A. M. Chamberlain, A. R. Chang, S. Cheng, S. R. Das, F. N. Delling, L. Djousse, M.S.V. Elkind, J. F. Ferguson, M. Fornage, L. C. Jordan, S. S. Khan, B. M. Kissela, K. L. Knutson, T. W. Kwan, D. T. Lackland, T.T. Lewis, J.H. Lichtman, C. T. Longenecker, M.S. Loop, P.L. Lutsey, S.S. Martin, K. Matsushita, A.E. Moran, M.E. Mussolini, M. O’Flaherty, A. Pandey, A. M. Perak, W. D. Rosamond, G.A. Rot, U.K.A. Sampson, G.M. Satou, E.B. Schroeder, S.H. Shah, N. L. Spartano, A. Stokes, D.L. Tirschwell, C.W. Tsao, M.P. Turakhia, L.B. VanWagner, J.T. Wilkins, S.S. Wong, and S. Virani. Heart disease and stroke statistics – 2019 update: A report from the american heart association. *Circulation*, 139:e56–e528, 2019.
- [3] B. Cansız, H. Dal, and M. Kaliske. Computational cardiology: A modified Hill model to describe the electro-visco-elasticity of the myocardium. *Computer Methods in Applied Mechanics and Engineering*, 315:434–466, 2017.
- [4] B. Cansız, H. Dal, and M. Kaliske. Computational cardiology: The bidomain based modified Hill model incorporating viscous effects for cardiac defibrillation. *Computational Mechanics*, 62:253–271, 2018.
- [5] B. Cansız, K. Sveric, K. Ibrahim, R. H. Strasser, A. Linke, and M. Kaliske. Towards predictive computer simulations in cardiology: Finite element analysis of personalized heart models. *Zeitschrift für Angewandte Mathematik und Mechanik*, 98:2155–2176, 2018.
- [6] F. B. C. Cansız, H. Dal, and M. Kaliske. An orthotropic viscoelastic material model for passive myocardium: Theory and algorithmic treatment. *Computer Methods in Biomechanics and Biomedical Engineering*, 18:1160–1172, 2015.
- [7] H. Dal, S. Göktepe, E. Kuhl, and M. Kaliske. A fully implicit finite element method for bidomain models of cardiac electrophysiology. *Computer Methods in Biomechanics and Biomedical Engineering*, 15:645–656, 2012.
- [8] H. Dal, S. Göktepe, E. Kuhl, and M. Kaliske. A fully implicit finite element method for bidomain models of cardiac electromechanics. *Computer Methods in Applied Mechanics and Engineering*, 253:323–336, 2013.
- [9] L.R. Garcia, B.F. Polegato, and L.A.M. Zornoff. Challenges of translational science. *Arquivos Brasileiros de Cardiologia*, 108:388–389, 2017.
- [10] S. Göktepe and E. Kuhl. Electromechanics of the heart: a unified approach to the strongly coupled excitation-contraction problem. *Computational Mechanics*, 45:227–243, 2010.
- [11] S. Göktepe, A. Menzel, and E. Kuhl. The generalized hill model: A kinematic approach towards active muscle contraction. *Journal of the Mechanics and Physics of Solids*, 72:20–39, 2014.
- [12] M. L. Gruber. The incidence of diagnostic error in medicine. *BMJ Quality & Safety*, 22:21–27, 2013.
- [13] A. V. Hill. The heat of shortening and the dynamic constants of muscle. *Proceedings of the Royal Society B: Biological Sciences*, 126:136–195, 1938.
- [14] P. Kohl, A. D. Nesbitt, P. J. Cooper, and M. Lei. Sudden cardiac death by commotio cordis: role of mechano-electric feedback. *Cardiovascular Research*, 50:280–289, 2001.
- [15] I. Medicine, B.H.S. Policy, D.T. Forum on Drug Discovery, R.B. Giffin, Y. Lebovitz, and R.A. English. *Transforming Clinical Research in the United States: Challenges and Opportunities: Workshop Summary*. Forum on Drug Discovery, Development, and Translation. National Academies Press, Washington, DC, 2010.
- [16] A. V. Panfilov, R. H. Keldermann, and M. P. Nash. Self-organized pacemakers in a coupled reaction-diffusion-mechanics system. *Physical Review Letters*, 95:258104–1–258104–4, 2005.
- [17] K. H. W. ten Tusscher, D. Noble, P. J. Noble, and A. V. Panfilov. A model for human ventricular tissue. *American Journal of Physiology-Heart and Circulatory Physiology*, 286:1573–1589, 2004.

Coupling cellular brain development with cortical folding

by Silvia Budday & Mohammad Saeed Zarzor

Chair of Applied Mechanics, Friedrich-Alexander-University Erlangen-Nürnberg, Germany

1 Abstract

In the early stages of human brain development, the initially smooth outer layer, the cortex, buckles into a highly convoluted pattern – driven by growth-induced mechanical instabilities. The cortical folding pattern is closely correlated with brain function. Therefore, malformations are an important clinical indicator for neurological disorders, such as schizophrenia or epilepsy. Computational mechanics is a powerful tool to understand the underlying mechanisms of cortical malformations and to assist diagnosis and treatment of associated diseases. This, however, will only become possible if we succeed in linking (disrupted) cellular brain development on the microscopic scale to (ab)normal cortical folding on the macroscopic scale. Here, we use a multifield computational framework, which couples an advection-diffusion model with finite growth, to model the complex interplay between cell division and migration, cellular connectivity, and cortical folding during physiological and pathological brain development.

2 Introduction

Throughout brain development, the complex structure of this fascinating organ keeps changing – on both microscopic and macroscopic scales – in close relation to brain function. Computational models based on the nonlinear field theories of mechanics are a promising tool to transfer processes on the cellular scale to structural changes on the continuum scale.

On the cellular scale, progenitor cells divide symmetrically and asymmetrically in the inner layers of our brain in the early stages of development [5, 23, 13]. The newly generated neurons deep inside the brain then migrate outwards along so-called radial glial cell (RGC) fibers, and finally form the cortex from the inside to the outside [22], as illustrated in Figure 1, left. RGC fibers control the migration direction of neurons. After about 20 weeks of gestation, the neuronal cells settled in the cortex start to interconnect, which initiates a significant expansion of the outer cortical brain layers. Not only neurons, but also other cellular components such as glial cells (astrocytes, oligodendrocytes, and microglial cells) and capillaries start to accumulate and grow [3] (Figure 1, right). The cortical expansion during neuronal connectivity is constrained by slower growing inner layers

[20]. Thus, compressive stresses emerge, which eventually induce mechanical instabilities and cortical folding [24, 4, 13]. If either cell migration or cellular connectivity are disrupted, cortical malformations can occur, which are associated with mental disorders including developmental delay, epilepsy, or schizophrenia [19, 2]. Computational mechanics can help to elucidate the underlying (physical) mechanisms of such diseases [13].

3 Computational model

3.1 Coupling cellular migration, cellular connectivity, and volume growth

We can model the (physiological and pathological) cortical folding process using the theory of finite growth [4, 12]. This common approach multiplicatively decomposes the deformation gradient \mathbf{F} into an elastic part \mathbf{F}^e and a growth part \mathbf{F}^g [25],

$$\mathbf{F} = \nabla_{\mathbf{X}} \varphi = \mathbf{F}^e \cdot \mathbf{F}^g \quad (1)$$

The key is then to prescribe the growth tensor \mathbf{F}^g and its evolution in time to realistically mimic the phenomena underlying growth in the developing brain. We assume that the cortex layer grows anisotropically during the phase of emerging neuronal connectivity. Therefore, we formulate the growth tensor as

$$\mathbf{F}^g = \vartheta^\perp [\mathbf{I} - \mathbf{N} \otimes \mathbf{N}] + \vartheta^\parallel \mathbf{N} \otimes \mathbf{N} \quad (2)$$

where \mathbf{N} denotes the outward pointing normal in the reference configuration \mathcal{B}_0 , and ϑ^\perp and ϑ^\parallel denote the scalar-valued growth multipliers controlling the amount of growth in the tangential and radial directions, respectively, as illustrated in Figure 2.

The balance of linear momentum forms the key equation to describe the deformation of the brain during cortical folding. Herein, we reformulate the stresses in terms of the elastic deformation \mathbf{F}^e computed from the growth tensor in equation (1). This constitutes the first balance equation of the coupled problem, which, in the spatial configuration \mathcal{B}_t , reads

$$\operatorname{div} \boldsymbol{\sigma}(\mathbf{F}^e) = 0. \quad (3)$$

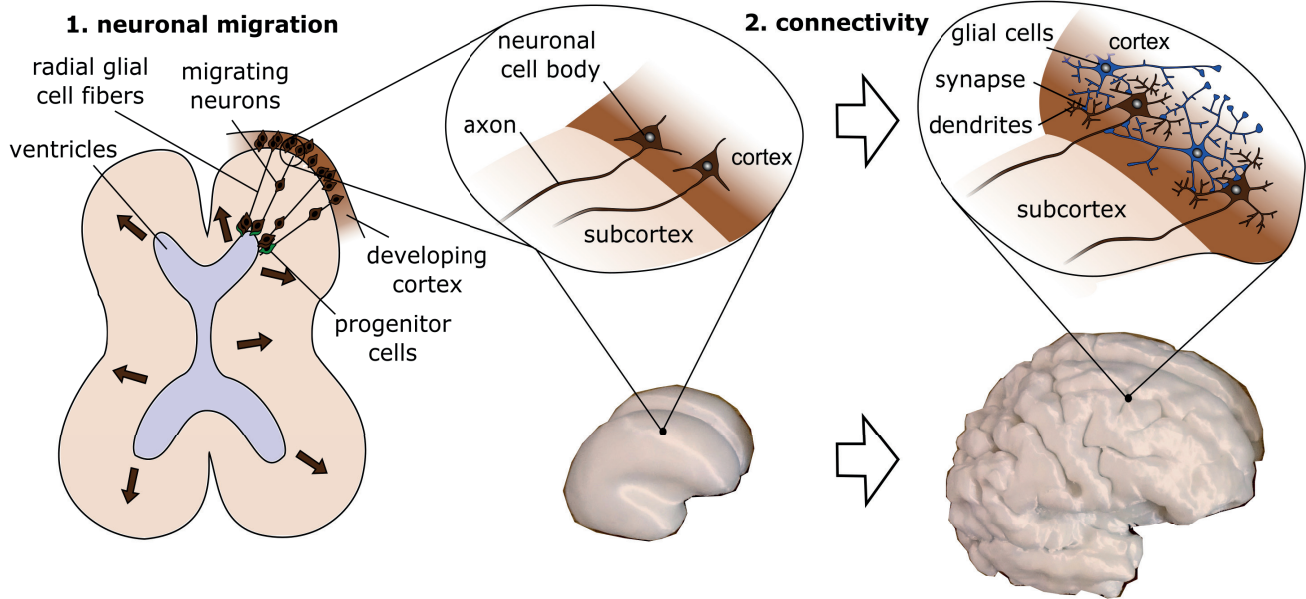


Figure 1: Schematic illustration of early brain development and neurogenesis, as well as neuronal connectivity resulting in cortical folding.

To link cellular processes, such as cell division in the inner brain layers, cell migration along radial glial cell fibers, and tangential migration of interneurons, with macroscopic growth and folding, recent studies have proposed to introduce the cell density as an additional scalar field c_0 , which is kept in balance through the cell density source R_c representing cell division, and the cell density flux \mathbf{Q}_c representing cell migration [28, 16].

We then additionally solve the balance of mass [17], which, in the reference configuration \mathcal{B}_0 , is given by

$$\dot{c}_0 = \text{Div } \mathbf{Q}_c + R_c, \quad (4)$$

while the corresponding equation in the spatial configuration \mathcal{B}_t reads

$$\frac{\partial}{\partial t} c + \dot{c} = \text{div } \mathbf{q}_c + r_c, \quad (5)$$

where J is the Jacobian $J = \det \mathbf{F}$, and \mathbf{q}_c and r_c are the spatial cell density flux and source, respectively [16]. We further couple the cell density problem with volume growth through a cell-density-dependent growth multiplier

$$\vartheta^\perp = [1 + \kappa^\perp c]^\alpha \quad \vartheta^{\parallel} = [1 + \kappa^{\parallel} c]^\alpha, \quad (6)$$

where κ^\perp and κ^{\parallel} denote the scalar-valued, spatially varying tangential and radial growth factors, and α denotes the growth exponent [16].

This approach enables us to explicitly predict how disruptions on the cellular level affect growth, folding, and structural abnormalities on the continuum scale.

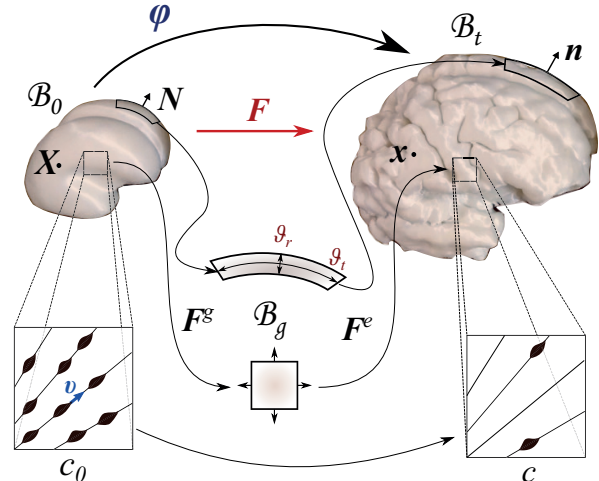


Figure 2: Kinematics of finite growth based on the multiplicative decomposition of the deformation gradient \mathbf{F} into an elastic part \mathbf{F}^e and a growth part \mathbf{F}^g . The deformation map ϕ maps tissue at position \mathbf{X} in the undeformed, ungrown reference configuration \mathcal{B}_0 to its new position $\mathbf{x} = \varphi(\mathbf{X}, t)$ in the spatial, grown and deformed configuration \mathcal{B}_t . The growth tensor \mathbf{F}^g maps tissue from the reference configuration to a stress-free configuration after growth \mathcal{B}_g and is coupled to cell division, migration and diffusion through cell-density-dependent tangential and radial growth multipliers ϑ^\perp and ϑ^{\parallel} , wherein the cell density c is introduced as an additional field with its reference distribution $c_0(\mathbf{X})$.

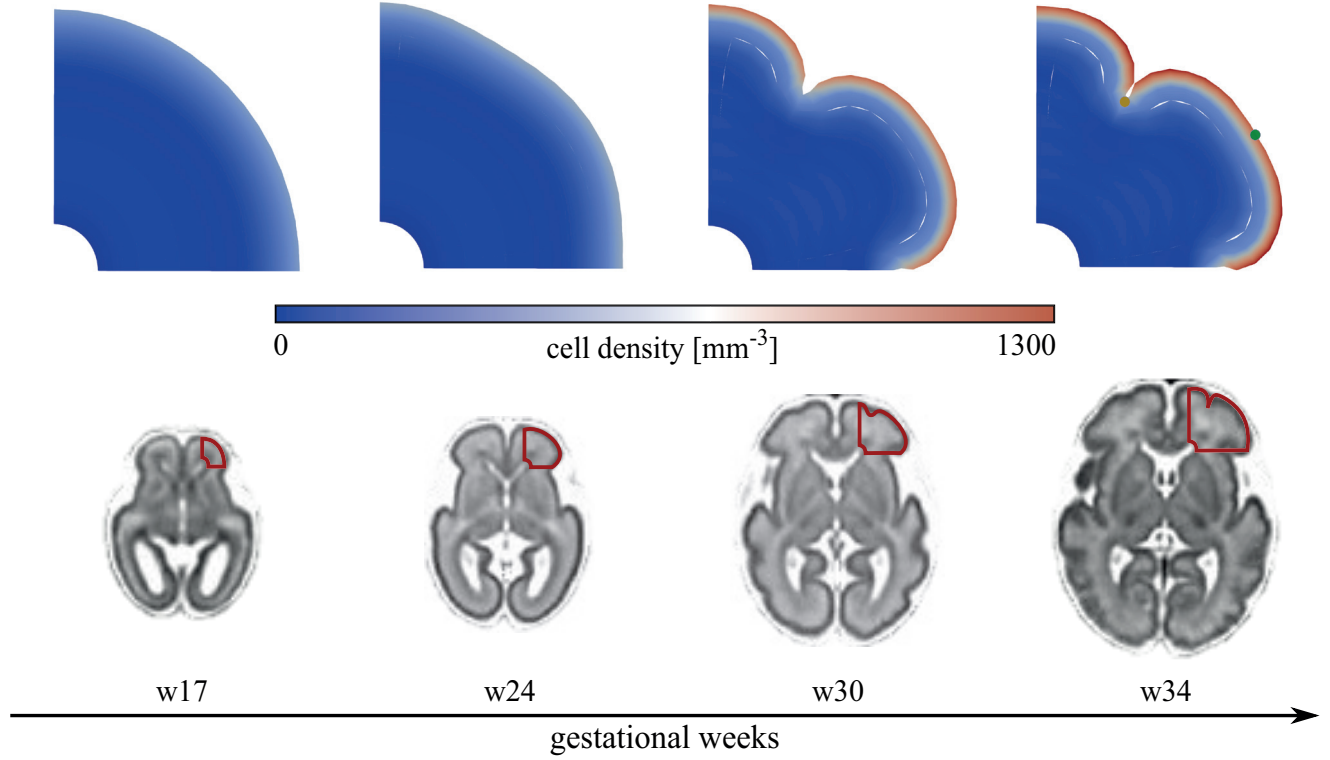


Figure 3: Exemplary evolution of the cell density field and cortical folding. The simulation (top row) well captures the evolving surface pattern shown on magnetic resonance images of the developing fetal brain (bottom row), adapted from [18].

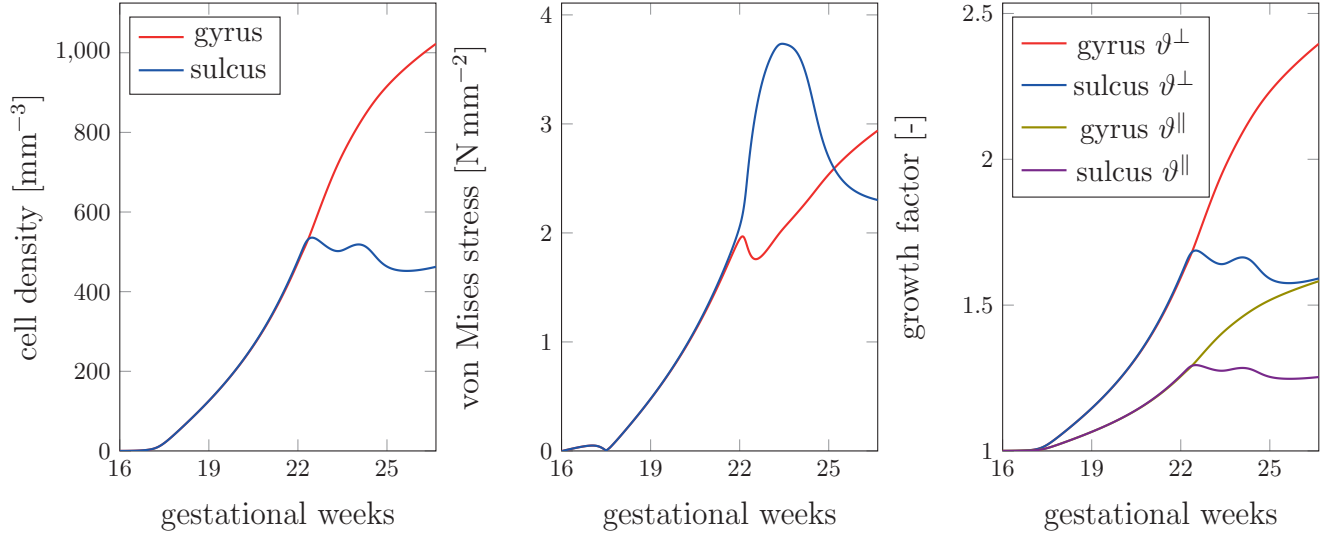


Figure 4: The temporal evolution of cell density, von Mises stress, radial, and tangential growth factors estimated at the green and yellow points in Figure 3 corresponding to gyri and sulci, respectively.

3.2 Constitutive equations

Mathematically, we formulate the flux term that appears in equations (4) and (5) by using a convection-diffusion

equation,

$$\mathbf{q}_c = -c \mathcal{H}(c; \gamma) \mathbf{v}(\mathbf{x}) + \mathbf{d}^{cc} \cdot \nabla_{\mathbf{x}} c, \quad (7)$$

where the reference and the spatial fluxes are related by $\mathbf{Q}_c = J\mathbf{q}_c \cdot \mathbf{F}^{-T}$ [15, 16]. The flux is a summation of two terms. The first term (migration term) represents the migration of the cells along the radial glial cell fiber direction towards the brain surface, as illustrated in Figures 1 and 2. The second term (diffusion term) represents cellular diffusion, which occurs when the neurons have reached the cortical layers [14]. The nonlinear Heaviside function $\mathcal{H}(c; \gamma) = \exp(\gamma(c - c^0)) / [1 + \exp(\gamma(c - c^0))]$, controls the distribution of the cell-density field, where c^0 is the migration threshold. The migration velocity $\mathbf{v} = v\mathbf{n}/\|\mathbf{n}\|$ defines the direction and speed of neuronal migration. Here, \mathbf{n} denotes the normalized radial glial cell fiber direction vector in the spatial configuration, as illustrated in Figure 2. The diffusion tensor $\mathbf{d}^{cc} = d^{cc} \mathbf{I}$ describes isotropic diffusion with diffusivity d^{cc} . The Jacobian links the reference source term to the spatial source term by $\mathbf{R}_c = J\mathbf{r}_c$. The cell division rate $G^c(\mathbf{x})$ defines the spatial source term

$$\mathbf{r}_c = G^c(\mathbf{x}). \quad (8)$$

Importantly, cellular rearrangements during brain development, as schematically shown in Figure 1, not only result in tissue growth but also in changes in tissue stiffness [29, 27]. This process has not yet been well assessed experimentally in humans and therefore constitutes a challenge when choosing appropriate material laws and material parameters to simulate brain development. Importantly, especially for cortical folding, the stiffness contrast between the different layers, cortex and subcortex, plays a key role and largely controls the evolving surface pattern and the mode of instability [12]. Here, we model brain tissue as a neo-Hookean hyperelastic solid with the strain-energy function

$$\begin{aligned} \psi(\mathbf{F}^e) = & \frac{1}{2} \lambda \ln^2(J^e) \\ & + \frac{1}{2} \mu [\mathbf{F}^e : \mathbf{F}^e - 3 - 2 \ln(J^e)], \end{aligned} \quad (9)$$

where μ and λ are the Lamé constants. To capture the varying stiffness due to tissue maturation in the developing brain, we introduce the shear modulus as a function of the cell density c ,

$$\mu(c) = \begin{cases} \mu_{\max} & \text{if } c \geq c_{\max}, \\ \mu_0 + m_c(c - c^0) & \text{if } c_{\max} > c > c^0, \\ \mu_0 & \text{if } c \leq c^0. \end{cases} \quad (10)$$

where μ_0 and μ_{\max} are the minimum and maximum shear moduli at the beginning and end of gestation, respectively, with corresponding cell densities c^0 and c_{\max} . The

cell density corresponding to the lowest shear modulus is equal to the migration threshold. The gradient m_c is computed as

$$m_c = \frac{\mu_{\max} - \mu_0}{c_{\max} - c^0}. \quad (11)$$

We note that this positive relation between cell density and brain tissue stiffness is only valid during the developmental phase [27], while the trend appears to be reversed in the fully developed brain [7]; it changes throughout the life cycle of the human brain [8].

4 Results

4.1 Spatio-temporal evolution of cell density, stiffness and cortical folding

To validate the computational model, we use a simple 2D problem representing a part of the frontal lobe of the human brain, as illustrated in Figure 3. We use the material parameters, which we obtained from biomechanical experiments of different regions of human brain tissue under multiple loading modes [10, 9]. Our study showed that the cortex is approximately three times stiffer than subcortical areas with a cortical shear modulus of 2.07 kPa and a subcortical modulus of approximately 0.65 kPa. As these values were measured in the fully developed brain—not during early stages of development—we have additionally systematically varied the stiffness ratio between the cortex and subcortex $\beta_\mu = \mu_c/\mu_s$ in the range of 3 and 10 to investigate its effect on the cortical folding pattern. We observed most realistic patterns for stiffness ratios between 3 and 5. An additional critical factor for the folding process is the growth ratio between tangential and radial growth $\beta_g = \kappa^\perp/\kappa^\parallel$ (see equation 6), which we have varied between $\beta_g = 1, 1.5$, and 3 . Table 1 summarizes all model parameters used for the simulation in Figure 3. Figure 3 contrasts the simulation results with magnetic resonance images of fetal brains published in [18]. The simulation well captures the evolution of cortical folds from week 17 until week 34 of gestation. Figure 4 shows the corresponding evolution of cell density, von Mises stress, as well as radial and tangential growth factors at a representative point in a gyrus and sulcus, respectively, marked as green and yellow points in Figure 3. The model predicts the known phenomenon that cell density and growth are lower in sulci than in gyri. Both show a pitchfork-like bifurcation at the initiation of cortical folding: the initially uniform distribution of cell nuclei and growth in the cortex starts to decrease in sulci, while it continues to increase in gyri. In contrast, the von Mises stress starts to drop in gyri at the instability point, but rises again after reach-

Table 1: Model parameters.

parameter		value	unit
cortical stiffness	μ_c	2.07	N mm ⁻²
stiffness ratio	β_μ	5	-
first Lamé parameter	λ	6.5	N mm ⁻²
division rate	G^c	130	mm ⁻² d ⁻¹
migration speed	v	5	mm d ⁻¹
migration threshold	c^0	400	mm ⁻³
Heaviside exponent	γ	0.008	-
diffusivity	d^{cc}	0.11	mm ² d ⁻¹
growth parameter	κ^\perp	7.05×10^{-4}	mm ²
growth exponent	α	1.65	-
growth ratio	β_g	1.5	-

ing a local minimum at around 29 weeks of gestation.

In the sulci, the stress reaches its maximum at around 31 weeks of gestation and then starts to decrease until it even drops below the stresses in gyri at around 34 gestational weeks.

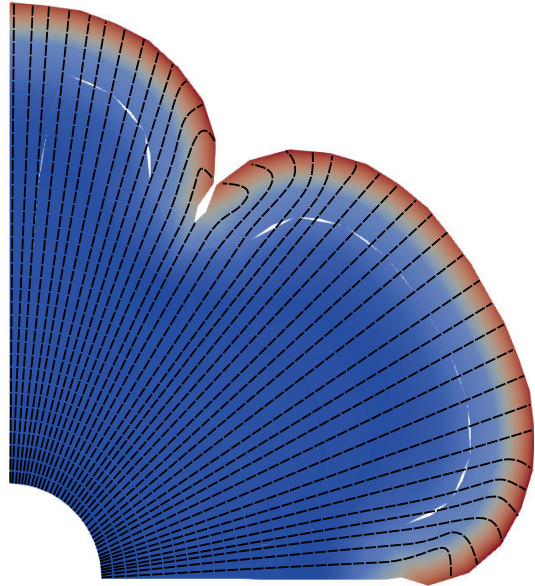


Figure 5: Numerically predicted orientation of radial glial cell fibers well resembles the fan-like structure known from the human brain.

Interestingly, our simulations suggest that certain features such as the fan-like distribution of radial glial cell fibers, which have been regarded as possible driving forces of cortical folding in the neuroscience community [6], are rather a result than a cause of the folding process, as numerically predicted in Figure 5. These insights demonstrate the value of coupling processes on the cellular level with cortical folding. Only then, it becomes

possible to connect knowledge from the neuroscience perspective with results from numerical analyses of cortical folding.

4.2 The effect of brain geometry

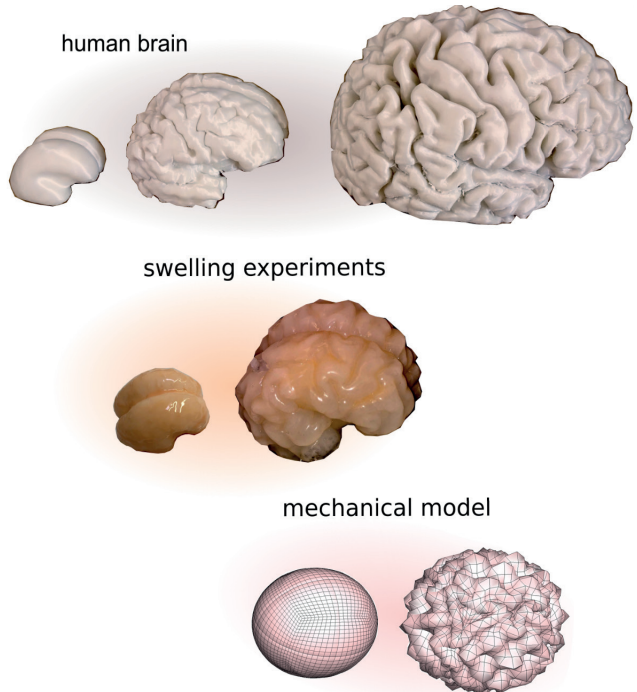


Figure 6: The three-dimensional cortical folding pattern in the developing human brain at gestational week 22, at birth, and at the age of 30 (top), compared to the swelling of a bilayered silicone elastomer (middle), and finite element simulations (bottom).

Besides stiffness and growth, geometrical factors, especially cortical thickness and local brain curvature, play an important role for the evolving folding pattern [11]. As it is difficult to obtain fine resolution three-dimensional data on the evolution of the brain's surface during devel-

opment in utero, we propose to use an experimental setup to further validate the computationally predicted folding patterns. We study the effects of abnormal brain shape, cortical thickness or brain stiffness through swelling experiments with silicon elastomers, where the outer layer representing the cortex swells when immersed in solvent [26]. Due to the constraint by the inner core representing the subcortex, folds emerge that closely resemble the morphology of the human brain at birth, as illustrated in Figure 6, middle. Through the combination of coupled simulations, swelling experiments, and imaging analyses of the human brain, our goal is to extract purely geometrical effects from cell programming and biological factors.

5 Conclusions and future perspectives

Computational mechanics have become a powerful tool to predict the structural development of the human brain. It may open new pathways where traditional medical approaches reach their limits. While the role of mechanics for brain function, injury, and disease is increasingly appreciated by neuroscientists, biologists and medical researchers, mechanical aspects have so far not been adopted to enhance daily clinical practice. In this respect, the current approach constitutes an important step to enable mechanics-enhanced diagnosis and treatment strategies in the future. Through the presented methodology, we aim to link the diagnostic findings on the microscopic scale, for instance from histological sections, with clinical data on the organ scale, e.g., from magnetic resonance images – to obtain unprecedented insights into diseases associated with brain malformations. To further calibrate and validate our simulations in the future, we are currently collaborating with neuropathologists, who will provide us with cell density distributions from histological stains at different stages of human brain development. In addition, future steps will include tackling neurological diseases such as epilepsy and modeling the active behavior of cells. Mechanical properties of their micro-environment affect cell migration, proliferation, and growth. In turn, the cells produce the extracellular matrix and therewith alter the mechanical properties of their environment. This leads to a highly coupled, yet very exciting problem. Modeling these processes computationally will revolutionize the opportunities to use simulations to advance diagnosis and treatment of neurological diseases or brain injury. While it will be challenging to accurately calibrate and validate such models, they may eventually help to find alternative identification criteria and treatment strategies for neurological disorders that are directly linked to malformations of cortical development, such as epilepsy, schizophrenia, or autism [1, 2].

Acknowledgements

We gratefully acknowledge the financial support by the German Research Foundation grant BU 3728/1-1, as well as the Emerging Talents Initiative (ETI) funding by the FAU. Furthermore, we would like to cordially thank Ingmar Blümcke for valuable discussions and Alexander Greiner for his tedious work on the swelling experiments.

References

- [1] Eleonora Aronica, Albert J Becker, and Roberto Spreafico. Malformations of cortical development. *Brain Pathol.*, 22(3):380–401, 2012.
- [2] A James Barkovich, Renzo Guerrini, Ruben I Kuzniecky, Graeme D Jackson, and William B Dobyns. A developmental and genetic classification for malformations of cortical development: update 2012. *Brain*, 135(5):1348–1369, 2012.
- [3] Ben A Barres. The mystery and magic of glia: a perspective on their roles in health and disease. *Neuron*, 60(3):430–440, 2008.
- [4] PV Bayly, RJ Okamoto, G Xu, Y Shi, and LA Taber. A cortical folding model incorporating stress-dependent growth explains gyral wavelengths and stress patterns in the developing brain. *Phys. Biol.*, 10(1):016005, 2013.
- [5] William T Blows. Child brain development. *Nurs. Times*, 99(17):28–31, 2003.
- [6] Víctor Borrell and Magdalena Gtz. Role of radial glial cells in cerebral cortex folding. *Current Opinion in Neurobiology*, 27:39–46, aug 2014.
- [7] S. Budday, M. Sarem, L. Starck, G. Sommer, J. Pfefferle, N. Phunchago, E. Kuhl, F. Paulsen, P. Steinmann, V.P. Shastri, and G.A. Holzapfel. Towards microstructure-informed material models for human brain tissue. *Acta Biomater.*, 104:53–65, mar 2020.
- [8] Silvia Budday and Ellen Kuhl. Modeling the life cycle of the human brain. *Curr. Opin. Biomed. Eng.*, 15:16–25, sep 2020.
- [9] Silvia Budday, Timothy C Ovaert, Gerhard A Holzapfel, Paul Steinmann, and Ellen Kuhl. Fifty shades of brain: A review on the mechanical testing and modeling of brain tissue. *Arch. Comput. Methods Eng.*, pages 1–44, 2019.
- [10] Silvia Budday, Gerhard Sommer, Christoph Birk, Christian Langkammer, Johannes Haybaeck, Julius Kohnert, Melanie Bauer, Friedrich Paulsen, Paul Steinmann, Ellen Kuhl, and Gerhard A. Holzapfel. Mechanical characterization of human brain tissue. *Acta Biomater.*, 48:319–340, 2017.

- [11] Silvia Budday, Paul Steinmann, Alain Goriely, and Ellen Kuhl. Size and curvature regulate pattern selection in the mammalian brain. *Extreme Mech. Lett.*, 4:193–198, 2015.
- [12] Silvia Budday, Paul Steinmann, and Ellen Kuhl. The role of mechanics during brain development. *J. Mech. Phys. Solids*, 72:75–92, 2014.
- [13] Silvia Budday, Paul Steinmann, and Ellen Kuhl. Physical biology of human brain development. *Front. Cell. Neurosci.*, 9:257, 2015.
- [14] VM Burlakov, R Taylor, J Koerner, and N Emptage. Analysis of microscopic parameters of single-particle trajectories in neurons. *Biophys. J.*, 99(5):1368–1376, 2010.
- [15] Brian N Cox and Chad M Landis. Solitary waves in morphogenesis: Determination fronts as strain-cued strain transformations among automatonous cells. *J. Mech. Phys. Solids*, 111:239–276, 2018.
- [16] Rijk de Rooij and Ellen Kuhl. A physical multi-field model predicts the development of volume and structure in the human brain. *J. Mech. Phys. Solids*, 112:563–576, 2018.
- [17] K Garikipati, Ellen M Arruda, K Grosh, H Narayanan, and S Calve. A continuum treatment of growth in biological tissue: the coupling of mass transport and mechanics. *J. Mech. Phys. Solids*, 52(7):1595–1625, 2004.
- [18] Ali Gholipour, Caitlin K. Rollins, Clemente Velasco-Annis, Abdelhakim Ouaalam, Alireza Akhondi-Asl, Onur Afacan, Cynthia M. Ortinau, Sean Clancy, Catherine Limperopoulos, Edward Yang, Judy A. Estroff, and Simon K. Warfield. A normative spatiotemporal MRI atlas of the fetal brain for automatic segmentation and analysis of early brain growth. *Scientific Reports*, 7(1), mar 2017.
- [19] Renzo Guerrini, William B Dobyns, and A James Barkovich. Abnormal development of the human cerebral cortex: genetics, functional consequences and treatment options. *Trends Neurosci.*, 31(3):154–162, 2008.
- [20] Peter R Huttenlocher and Arun S Dabholkar. Regional differences in synaptogenesis in human cerebral cortex. *J. Comp. Neurol.*, 387(2):167–178, 1997.
- [21] Ellen Kuhl and Paul Steinmann. Mass-and volume-specific views on thermodynamics for open systems. *Proc. R. Soc. A*, 459(2038):2547–2568, 2003.
- [22] Pasko Rakic. Specification of cerebral cortical areas. *Science*, 241(4862):170–176, 1988.
- [23] Charles Raybaud, Tahani Ahmad, Neda Rastegar, Manohar Shroff, and Mutaz Al Nassar. The premature brain: developmental and lesional anatomy. *Neuroradiology*, 55(2):23–40, 2013.
- [24] David P Richman, R Malcolm Stewart, JW Hutchinson, and Verne S Caviness Jr. Mechanical mode of brain convolutional development. *Science*, 189:18–21, 1975.
- [25] Edward K Rodriguez, Anne Hoger, and Andrew D McCulloch. Stress-dependent finite growth in soft elastic tissues. *J. Biomech.*, 27(4):455–467, 1994.
- [26] Tuomas Tallinen, Jun Young Chung, François Rousseau, Nadine Girard, Julien Lefèvre, and L Mahadevan. On the growth and form of cortical convolutions. *Nat. Phys.*, 12(6):588–593, 2016.
- [27] Amelia J Thompson, Eva K Pillai, Ivan B Dimov, Sarah K Foster, Christine E Holt, and Kristian Franze. Rapid changes in tissue mechanics regulate cell behaviour in the developing embryonic brain. *eLife*, 8:e39356, 2019.
- [28] SN Verner and K Garikipati. A computational study of growth-driven folding patterns on shells, with application to the developing brain. *arXiv preprint arXiv:1709.05546*, 2017.
- [29] Johannes Weickenmeier, Rijk de Rooij, Silvia Budday, Timothy C Ovaert, and Ellen Kuhl. The mechanical importance of myelination in the central nervous system. *J. Mech. Behav. Biomed. Mater.*, 76:119–124, 2017.

Computational Modeling of the Stomach

by Roland C. Aydin¹, Roustem N. Miftahof², Sebastian Brandstaeter³, Sebastian L. Fuchs^{2,3} & Christian J. Cyron^{1,2}

¹ Institute of Materials Research, Materials Mechanics, Helmholtz-Zentrum Geesthacht, Germany

² Institute of Continuum and Materials Mechanics, Hamburg University of Technology, Germany

³ Institute for Computational Mechanics, Technical University of Munich, Germany

1 Abstract

In computational biomechanics, the gastro-intestinal tract (stomach and intestine) is much less studied than the cardio-vascular system. The focus on the cardio-vascular system is most likely a consequence of its vital importance, whereas gastro-intestinal pathologies often result in a substantial and permanent reduction of the quality of life but are in many cases not deadly. However, as life expectancy keeps increasing, quality of life is becoming more and more important. Hence, we can expect that the gastro-intestinal tract will attract more and more attention over the next years. In this article, we briefly summarize the state of the art and highlight opportunities for computational researchers in this emerging area of computational biomechanics.

2 Introduction

Pathologies related to the gastro-intestinal tract are a frequent cause of morbidity with an associated high economic cost and substantial reduction of the quality of life. For example, gastro-esophageal reflux disease (GERD) causes an estimated \$20 billion/year of healthcare costs in the US alone [14]. At the same time, in the general population of industrialized countries 10% - 45% are assumed to suffer from dyspepsia (indigestion) [23], and the soaring prevalence of obesity has resulted in hundred thousands of bariatric surgeries per year in the US and EU together [5, 1]. All these issues are closely related to the mechanics of the stomach. At the same time, nobody has yet proposed a computational multi-physics model of the stomach combining at least the most important aspects of its mechanics, that is, the fluid mechanics of the digesta and the electromechanics of the gastric wall in a comprehensive computational framework. This limitation of the state of the art can be understood as a great opportunity for researchers from computational mechanics. In the following, we give a brief introduction to the state of the art in computational gastric mechanics and highlight promising opportunities in this field for researchers from computational mechanics.

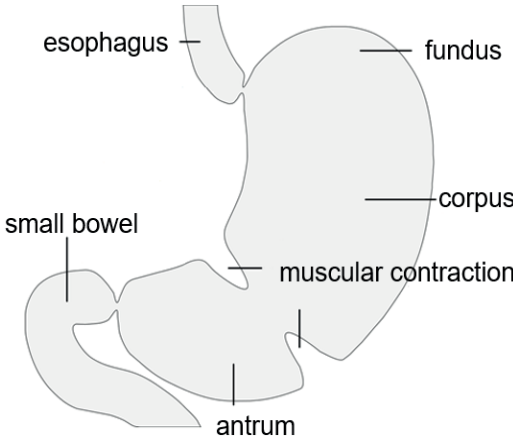


Figure 1: The stomach is located between esophagus and small bowel and can be divided into three regions, fundus, corpus, and antrum. Whereas the fundus mainly serves for storing digesta, corpus and antrum are responsible for mixing and grinding them by muscular contraction waves that originate in the upper (proximal) part of the stomach and propagate towards the pylorus, which is separating the stomach from the small bowel; illustration created by Christian J. Cyron and Roland C. Aydin, licensed under CC BY 4.0 (creativecommons.org/licenses/by/4.0/legalcode)

Anatomically, the stomach connects the esophagus and the intestine. Food arrives through the mouth and esophagus in the stomach. The stomach is storing, mixing, and grinding the digesta before they are passed for further digestion through the pylorus into the small intestine. The stomach is a roughly J-shaped hollow muscular organ (Figure 1), filled with a fluid-like content, the digesta. The mechanics of the wall of the stomach is formed by living tissue and exhibits both a passive elasticity and an active muscular tension. The digesta arrive in the stomach in the form of still solid-like food boluses and are subsequently degraded and diluted in the liquid environment of the stomach until they form a multi-phase fluid. This process is promoted by rhythmic muscular contractions of the stomach, so-called peristaltic waves moving along the stomach. These are controlled by slow electric waves propagating along the stomach. Thus, computational modeling of the stomach touches a number of different issues complex in nature. The related key questions are, how to model the

1. (passive) elasticity of the gastric wall,
2. propagation and effect of electric waves in the gastric wall,
3. (active) muscle tension in the gastric wall,
4. both solid and liquid phases of the digesta in the stomach,
5. interactions between the digesta and the gastric wall.

In the subsequent sections, the state of the art with respect to these five key questions as well as open problems are discussed.

3 Elasticity of the gastric wall

The mechanical properties of the stomach wall are highly specific. They are affected by environmental factors and age. Like many biological tissues, the gastric wall exhibits a highly nonlinear and anisotropic elastic behavior. It can be modeled by a nonlinear strain energy function W . With the deformation gradient \mathbf{F} , Cauchy stress can then be computed as

$$\mathbf{T} = \frac{1}{\det(\mathbf{F})} \frac{\partial W}{\partial \mathbf{F}} \mathbf{F}^T. \quad (1)$$

For a discussion of appropriate strain energy functions and constitutive parameters for the gastric wall, the reader is referred to [17, 18, 19, 3, 12, 4]. Generally, the elastic properties of gastric tissue greatly vary between the three major regions of the stomach, the fundus, the corpus, and the antrum (Figure 1). To date, most available data about the elastic properties of gastric tissues come from animal tissues, and there remains in particular a need for more mechanical tests of human gastric tissue. These may help to understand whether or how changes in the elasticity of the gastric wall are related to pathologies such as dyspepsia or morbid obesity.

4 Electric waves in the gastric wall

For mixing and grinding the digesta, slow muscular contractions waves are propagating through the stomach, so-called peristaltic contractions. These are controlled by slow electric waves initiating in the upper (proximal) part of the stomach and propagating towards the pylorus with a frequency of around 3 cycles per minute. The electric waves are governed by a biological system that is by far more complex than the one controlling the contractions of the heart. This system relies on a complex interplay between smooth muscle cells (SMC) and the so-called interstitial cells of Cajal (ICC) [9, 25, 28]. Based

on homogenization techniques [13], continuum reaction-diffusion models of gastric electrical activity of varying complexity can be derived [2, 24, 8, 26, 10]. [7] showed that the following simple so-called monodomain model is sufficient to reproduce at least the most important patterns of slow electric wave initiation and propagation in the gastric wall on the continuum level:

$$\frac{\partial v^i}{\partial t} = \sigma^i \Delta v^i + I_{ion}^i - I_{gap}, \quad (2)$$

$$\frac{\partial v^m}{\partial t} = \sigma^m \Delta v^m + I_{ion}^m + I_{gap}. \quad (3)$$

Here, v^i , v^m are the electric transmembrane potentials of ICC and SMC, respectively, σ^i , σ^m denote isotropic diffusion parameters for the electrical potential in these two components of the tissue, Δ is the Laplace operator, and I_{ion}^i , I_{ion}^m and I_{gap} are electric currents. To compute these currents, either simple phenomenological equations or complex scale-bridging models relating cellular and organ level can be used. The development of such scale-bridging models is an active field of research and will probably remain so for at least the next decade. Computational modeling can be expected to be a powerful tool to develop and validate hypotheses in this area. To this end, a good starting point is the biophysical model of gastrointestinal electrical activity developed by [22, 21]. The simulation of stable ring-shaped conduction patterns with the above-mentioned simple phenomenological model of slow electric wave initiation and propagation is illustrated in Figure 2 and Figure 3 (upper row) for a simple cylindrical gastric model geometry. The above-mentioned model can also produce perturbed propagation patterns that may help to understand gastric dysrhythmias and thus perhaps also dyspepsia (Figure 3, lower row).

5 Active muscle tension in the wall

The electric slow waves propagating through the stomach are controlling smooth muscle tension in the gastric wall through complex cellular processes where free intracellular $Ca^{(2+)}$ ions play a key role [16, 25]. The resulting muscular (peristaltic) contractions are mixing and grinding the digesta. Theoretical and experimental investigations of active SMC tension in the gastric wall is challenging. Only recently have the active mechanical properties of gastric smooth muscle tissue been studied for the first time in detail in experiments [27]. To model active tension in the gastric wall, two major approaches have been developed, the active stress and the active strain approach. In the active stress approach, the total stress in the gastric wall is computed as the sum of an elastic stress following Eq. (1) and an additional active muscular stress [16]. By contrast, in the active strain approach, the deformation gradient \mathbf{F} of the gastric wall

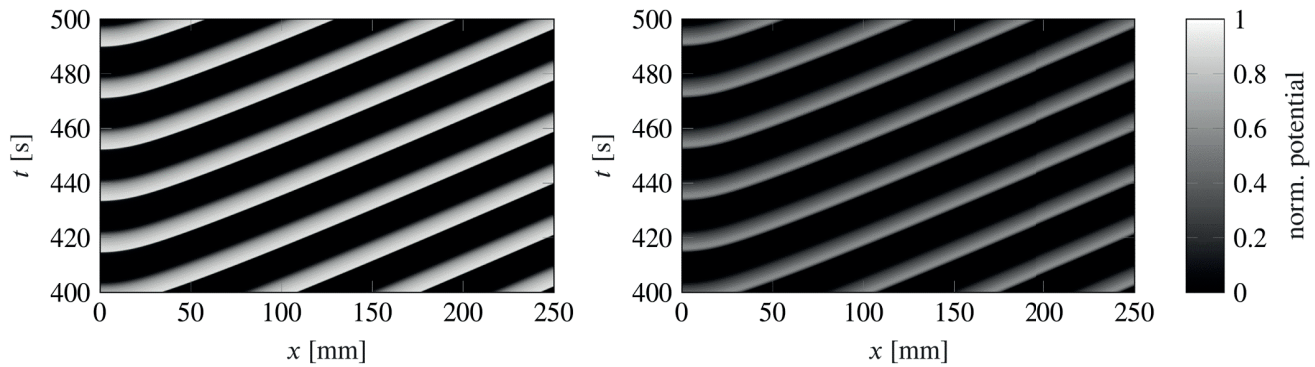


Figure 2: Spatiotemporal plot of slow electrical wave propagation in ICC (left) and SMC (right) in a one-dimensional domain used for testing purposes. Slow waves in SMC follow the excitation by ICC with a small delay and reduced amplitude; adapted from [7], licensed under CC BY 4.0 (creativecommons.org/licenses/by/4.0/legalcode).

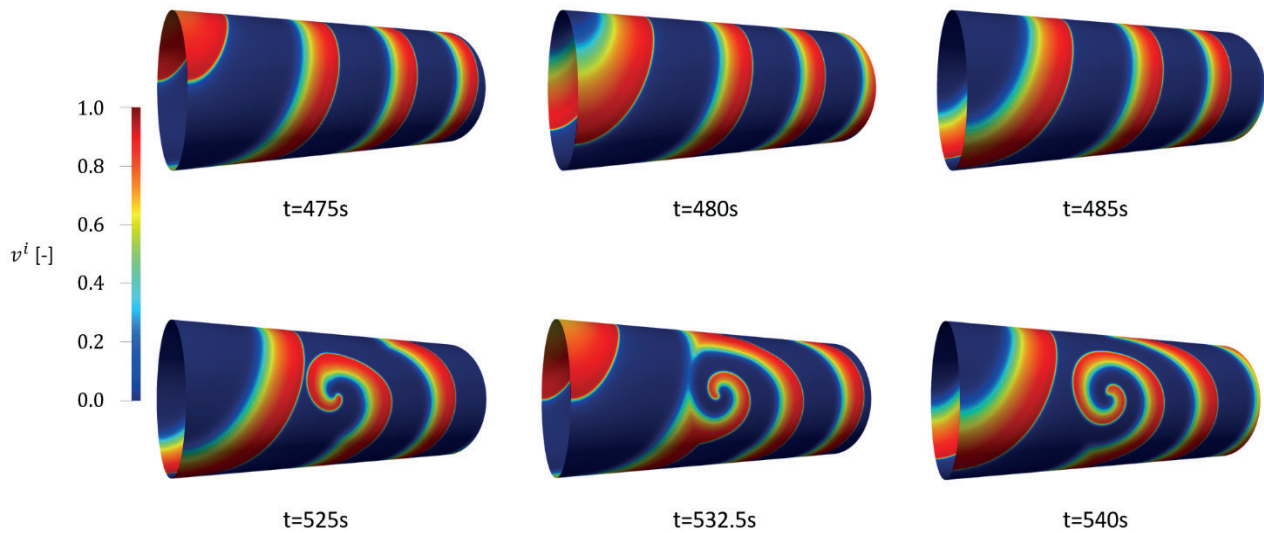


Figure 3: Generation and propagation of stable ring-shaped slow electric waves in ICC on an idealized cylindrical stomach geometry (upper row). At $t=500$ s, a perturbation of gastric electrophysiology modeling, for example, a pathological change of the gastric wall, is simulated by the addition of a conduction block. It results in the formation of a spiral-like pattern (lower row) and associated disordered peristaltic contractions of the stomach; illustration created by Christian J. Cyron and Sebastian Brandstaeter, licensed under CC BY 4.0 (creativecommons.org/licenses/by/4.0/legalcode)

can be decomposed multiplicatively via

$$\mathbf{F} = \mathbf{F}_e \mathbf{F}_a \quad (4)$$

into an inelastic part \mathbf{F}_a representing the load-free state of the tissue in the presence of a certain muscular tension, and a remaining elastic part \mathbf{F}_e . The latter ensures geometric compatibility of the deformation of the stomach as a whole, and the strain energy W in Eq. (1) solely depends on this elastic part. The first active strain model of the gastric wall stress was introduced by [7], using

$$\mathbf{F}_a = \mathbf{I} - \gamma(\alpha_c \mathbf{N}_c \otimes \mathbf{N}_c + \alpha_l \mathbf{N}_l \otimes \mathbf{N}_l) + \gamma_n \mathbf{N}_n \otimes \mathbf{N}_n. \quad (5)$$

Here, \mathbf{N}_c , \mathbf{N}_l and \mathbf{N}_n are the circumferential, longitudinal and wall-thickness direction of the gastric wall, respectively, and α_c , α_l are material parameters. The excitation-contraction coupling is realized by the activation parameter γ via a Heaviside-type function $\gamma = \gamma(v^m)$, where γ_n ensures incompressibility of the tissue under contraction. A finite element simulation of the gastric wall as a coupled system including the propagation of electric slow waves, the passive elasticity, and the active muscular tension (controlled by the electric slow waves) is presented in Figure 4. For more detailed models of the active muscle tension in the gastro-intestinal wall, the reader is referred to [20, 15].

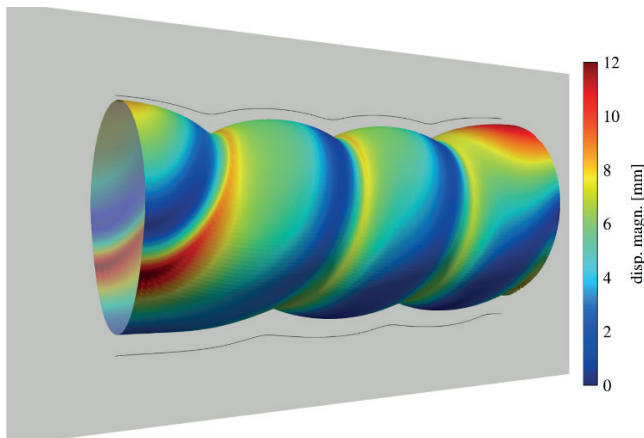


Figure 4: Computational active strain electromechanical model of an idealized cylindrical stomach geometry showing travelling phasic contraction waves of peristalsis, adapted from [7], licensed under CC BY 4.0 (creativecommons.org/licenses/by/4.0/legalcode)

6 Multi-phase flow of digesta

Mixing and grinding of the digesta in the stomach has been simulated so far only on the basis of highly simplified Newtonian or Non-Newtonian fluid models [11]. In reality, however, digesta are typically complex multiphasic materials consisting of one or several fluid phases as well as of one or several solid phases, for example,

food particles that are mechanically and chemically degraded in the stomach. Computational modeling of these aspects can help to understand the mechanical aspects and possibly also origins of certain gastric pathologies. It appears that much could be achieved in the future in this area of biomechanics by simply transferring progress that has been made in other areas of computational fluid mechanics over the past two decades to the specific problem of gastric mechanics.

7 Fluid-structure interactions

So far there is only a very limited number of studies of the fluid mechanics of the digesta in the stomach. These studies are not only limited to simple fluid models but additionally they all prescribe the motion of the gastric wall in a rigid form. Fluid-structure interactions between the digesta and the elastic gastric wall have not yet been modeled. It is well-known that these play key roles in the process of digestion in general and also in the complex hormonal control loops regulating food intake in particular. However, computational modeling of fluid-structure interactions in the stomach is much more challenging than, for example, in arteries or also the heart. The reasons for this are the extreme deformations of the stomach during ingestion and digestion of food and moreover also the above-mentioned multi-phase character of the digesta. The development of computational models overcoming these difficulties is a promising area of investigation for researchers with a strong background in fluid-structure interactions and computational fluid dynamics.

8 Conclusions

While the importance of the gastro-intestinal tract for healthcare is in many aspects comparable to the one of the cardio-vascular system, the research efforts spent on the latter by far surpass the ones spent on the former. One of the reasons is most likely the direct relation of the heart and blood vessels to mortality against which the enduring morbidity often caused by gastro-intestinal pathologies is often neglected. As a consequence, computational modeling of the stomach is so far one of the most underrated fields of computational biomechanics. Thus, for researchers with a background in computational mechanics it offers rich opportunities. In the domain of solid mechanics, these are mainly related to the development of multi-scale models relating cellular to continuum-scale processes. In the domain of fluid mechanics, modeling the multi-phase flow of the digesta as well as fluid-structure interactions between the digesta and the gastric wall are promising areas of research. Computer simulations of these aspects can not only help to understand

certain physiological foundations of our digestion and pathologies related to it for the first time but also form the basis for software tools that may be used in future computer-assisted bariatric surgeries. For a comprehensive review of the state of the art in gastric mechanics, the reader is referred to [6].

Acknowledgements

Funded by the Deutsche Forschungsgemeinschaft (DFG, German Research Foundation) – Projektnummer 350481011

References

- [1] Estimate of bariatric surgery numbers, 2011–2018. <https://asmbs.org/resources/estimate-of-bariatric-surgery-numbers>. Accessed: 2020-05-05.
- [2] R. R. Aliev, W. Richards, and J. P. Wikswo. A simple nonlinear model of electrical activity in the intestine. *Journal of Theoretical Biology*, 204(1):21–28, 2000.
- [3] R. C. Aydin, S. Brandstaeter, F. A. Braeu, M. Steigerberger, R. P. Marcus, K. Nikolaou, M. Notohamiprodjo, and C. J. Cyron. Experimental characterization of the biaxial mechanical properties of porcine gastric tissue. *Journal of the Mechanical Behavior of Biomedical Materials*, 74:499–506, 2017.
- [4] M. Bauer, E. Morales-Orcajo, L. Klemm, R. Seydewitz, V. Fiebach, T. Siebert, and M. Böhl. Biomechanical and microstructural characterisation of the porcine stomach wall: Location- and layer-dependent investigations. *Acta Biomaterialia*, 102:83–99, 2020.
- [5] O. Borisenco, Z. Colpan, B. Dillemans, P. Funch-Jensen, J. Hedenbro, and A.R. Ahmed. Clinical Indications, Utilization, and Funding of Bariatric Surgery in Europe. *Obesity Surgery*, 25(8):1408–1416, 2015.
- [6] S. Brandstaeter, S.L. Fuchs, R.C. Aydin, and C.J. Cyron. Mechanics of the stomach: A review of an emerging field of biomechanics. *GAMM-Mitteilungen*, 42(3):e201900001, 2019.
- [7] S. Brandstaeter, A. Gizzi, S.L. Fuchs, A.M. Gebauer, R.C. Aydin, and C.J. Cyron. Computational model of gastric motility with active-strain electromechanics. *ZAMM - Journal of Applied Mathematics and Mechanics / Zeitschrift für Angewandte Mathematik und Mechanik*, 98(12):2177–2197, 2018.
- [8] A. Corrias, P. Du, and M.L. Buist. Modelling tissue electrophysiology in the gi tract: past, present and future. In *New Advances in Gastrointestinal Motility Research*, pages 167–195. Springer, 2013.
- [9] B.T. Drumm, T.S. Sung, H. Zheng, S.A. Baker, S.D. Koh, and K.M. Sanders. The effects of mitochondrial inhibitors on Ca²⁺ signalling and electrical conductances required for pacemaking in interstitial cells of Cajal in the mouse small intestine. *Cell Calcium*, 72:1–17, 2018.
- [10] P. Du, S. Calder, T.R. Angeli, S. Sathar, N. Paskaranandavadiel, G. O’Grady, and L.K. Cheng. Progress in Mathematical Modeling of Gastrointestinal Slow Wave Abnormalities. *Frontiers in physiology*, 8:1136, 2018.
- [11] M.J. Ferrua, Z. Xue, and R. Paul Singh. On the kinematics and efficiency of advective mixing during gastric digestion - A numerical analysis. *Journal of biomechanics*, 47(15):3664–3673, 2014.
- [12] C.G. Fontanella, C. Salmaso, I. Toniolo, N. de Cesare, A. Rubini, G. M. de Benedictis, and E.L. Carniel. Computational Models for the Mechanical Investigation of Stomach Tissues and Structure. *Annals of biomedical engineering*, 47(5):1237–1249, 2019.
- [13] P.C. Franzone, L.F. Pavarino, and S. Scacchi. *Mathematical cardiac electrophysiology*. Springer, 2014.
- [14] A.J. Gawron, D.D. French, J.E. Pandolfino, and C.W. Howden. Economic Evaluations of Gastroesophageal Reflux Disease Medical Management: A Systematic Review. *PharmacoEconomics*, 32(8):745–758, 2014.
- [15] L. Klemm, R. Seydewitz, M. Borsdorf, T. Siebert, and M. Böhl. On a coupled electro-chemomechanical model of gastric smooth muscle contraction. *Acta biomaterialia*, 2020.
- [16] R.N. Miftahov. *Biomechanics of the human stomach*. Springer, 2017.
- [17] R.N. Miftakhov. Age-related changes of the mechanical properties of human gastric tissue. In *Shell Interactions with Fluids*, pages 197–204. Academy of Sciences of the USSR (in Russian) Moscow, 1981.
- [18] RN Miftakhov. Investigation of the human stomach tissue in uniaxial loading. *Hydroelasticity of Shells*, pages 163–171, 1983.
- [19] RN Miftakhov. Experimental investigation of the stomach tissue in biaxial loading. *Investigations in the Theory of Plates and Shells*, pages 35–46, 1985.

- [20] R.N. Miftakhov and G.R. Abdusheva. Numerical simulation of excitation-contraction coupling in a locus of the small bowel. *Biological cybernetics*, 74(5):455–467, 1996.
- [21] R.N. Miftakhov, G.R. Abdusheva, and J. Christensen. Numerical simulation of motility patterns of the small bowel. 1. Formulation of a mathematical model. *Journal of theoretical biology*, 197(1):89–112, 1999.
- [22] R.N. Miftakhov, G.R. Abdusheva, and J. Christensen. Numerical simulation of motility patterns of the small bowel. II. Comparative pharmacological validation of a mathematical model. *Journal of theoretical biology*, 200(3):261–290, 1999.
- [23] P. Oustamanolakis and J. Tack. Dyspepsia: organic versus functional. *Journal of clinical gastroenterology*, 46(3):175–190, 2012.
- [24] A. Pullan, L. Cheng, R. Yassi, and M. Buist. Modelling gastrointestinal bioelectric activity. *Progress in biophysics and molecular biology*, 85(2-3):523–550, 2004.
- [25] K.M. Sanders. Nerves, smooth muscle cells and interstitial cells in the GI tract: Molecular and cellular interactions. In *Clinical and Basic Neurogastroenterology and Motility*, pages 3–16. Elsevier, 2020.
- [26] S. Sathar, M.L. Trew, G. O’Grady, and L.K. Cheng. A Multiscale Tridomain Model for Simulating Bioelectric Gastric Pacing. *IEEE transactions on biomedical engineering*, 62(11):2685–2692, 2015.
- [27] A. Tomalka, M. Borsdorf, M. Bölk, and T. Siebert. Porcine Stomach Smooth Muscle Force Depends on History-Effects. *Frontiers in physiology*, 8(OCT):1–12, 2017.
- [28] H. Zheng, B.T. Drumm, M.H. Zhu, Y. Xie, K.E. O’Driscoll, S.A. Baker, B.A. Perrino, S.D. Koh, and K.M. Sanders. Na⁺/Ca²⁺ exchange and pacemaker activity of interstitial cells of Cajal. *Frontiers in Physiology*, 11(March):1–19, 2020.

gacm German Association for
Computational Mechanics

Institut für Statik und Dynamik der Tragwerke
Technische Universität Dresden

01062 Dresden

Phone: +49 351-463-35738

Fax: +49 351-463-37086

email: gacm@mailbox.tu-dresden.de

Internet: www.gacm.de